Research Square

Preprints are preliminary reports that have not undergone peer review.
They should not be considered conclusive, used to inform clinical practice,
or referenced by the media as validated information.

The Gut Microbiota/Gut Brain/BDNF Axis: A Mechanistically Defined Pathway Mediating the Neuroprotective Effects of Ginsenoside Re in Parkinson's Disease

Mengjie Tang
Changchun University of Chinese Medicine
Fangyuan Zhang
Changchun University of Chinese Medicine
Ziqi Liang
Shanghai University of Traditional Chinese Medicine
Jing Tian
Changchun University of Chinese Medicine
Dean Guo
Shanghai University of Traditional Chinese Medicine
Jiyu Gong
Changchun University of Chinese Medicine
Wenyi Gao
Changchun University of Chinese Medicine
Zizhao Yang
zzyang@shutcm.edu.cn

Shanghai University of Traditional Chinese Medicine

Article

Keywords: Gut Brain Axis, Parkinson's Disease (PD), Brain Derived Neurotrophic Factor (BDNF), Gut Microbiota, Ginsenoside Re (GsRe), TLR4 Pathway.

Posted Date: May 29th, 2026

DOI: https://doi.org/10.21203/rs.3.rs-9639310/v1

License: This work is licensed under a Creative Commons Attribution 4.0 International License.
Read Full License

Additional Declarations: No competing interests reported.

Version of Record: A version of this preprint was published at npj Science of Food on November 18th, 2026. See the published version at https://doi.org/10.1038/s41538-026-01210-x.

Abstract

Ginseng, as a traditional natural food and edible resource, has shown potential in the treatment of neurodegenerative diseases, particularly Parkinson's disease (PD), through its active components, ginsenosides (GS) and ginsenoside Re (GsRe). This study aimed to systematically investigate the neuroprotective effects and molecular underpinnings of total GS and GsRe in a 1-methyl-4-phenyl-1,2,3,6-tetrahydropyridine (MPTP) induced PD mouse model, with a focus on gut brain axis modulation. The results showed that, GS and GsRe ameliorated motor deficits, reduced substantia nigra pars compacta (SNpc) dopaminergic neuron loss, restored intestinal barrier integrity, and reversed gut dysbiosis. Mechanistically, GsRe crossed the BBB, upregulated brain derived neurotrophic factor (BDNF), and inhibited the TLR4 adaptor WDFY1, blocking excessive NF-κB activation, M1 microglial polarization, and neuronal apoptosis. BDNF deficiency exacerbated TLR4 pathway hyperactivation, confirming BDNF's upstream regulatory role. GS and GsRe target the gut brain axis as an integrated hub: normalizing gut microecology to limit peripheral inflammatory signal translocation, while suppressing central neuroinflammation via the BDNF/TLR4 axis. These findings provide a mechanistic basis for GS and GsRe based PD interventions, bridging gut dysbiosis and central neuroinflammation through a dual targeting strategy.

1. Introduction

Parkinson's disease (PD) is a progressive neurodegenerative disorder pathologically defined by the selective degeneration of dopaminergic neurons in the substantia nigra pars compacta (SNpc) and their striatal projections, accompanied by the accumulation of misfolded α-synuclein (α-syn, encoded with gene *SNCA*) into Lewy bodies and Lewy neurites[1,2]. Although levodopa remains the most effective symptomatic therapy for PD, it fails to modify underlying neurodegeneration and is frequently complicated by motor fluctuations and dyskinesias after prolonged administration[3]. Therefore, there is an urgent unmet need for disease modifying therapies that simultaneously target multiple pathogenic nodes, including α-syn aggregation, neuroinflammation, mitochondrial dysfunction, and gut brain axis disruption, to confer robust neuroprotection in PD.

The pathogenesis of PD is highly complex, and an imbalance between neurotrophic support and neuroinflammatory signaling represents a central pathogenic axis driving dopaminergic neuron degeneration. Brain derived neurotrophic factor (BDNF), a key neurotrophin critical for the survival, functional maintenance, and synaptic integrity of midbrain dopaminergic neurons, is consistently reduced in PD patients and preclinical models[4], is closely linked to the pathological mechanisms of PD[5]. BDNF downregulation alleviates transcriptional repression of the *SNCA* gene, leading to increased α-syn expression and subsequent pathological aggregation[6,7]. Moreover, BDNF deficiency downregulates tyrosine hydroxylase (TH) expression, the rate limiting enzyme in dopamine biosynthesis, thereby compromising dopaminergic neurotransmission through reduced dopamine synthesis, diminished neuronal excitability, and impaired vesicular release[8,9]. Regarding neuroinflammation, members of the

Toll like receptor (TLR) family, particularly TLR4, serve as critical pattern recognition receptors that detect damage associated molecular patterns (DAMPs) and pathogen associated molecular patterns (PAMPs), thereby initiating and sustaining microglia driven neuroinflammatory responses in PD[10]. In MPTP induced PD models, genetic or pharmacological TLR4 inhibition attenuates striatal dopamine depletion, restores TH and dopamine transporter (DAT) expression in the SNpc and striatum, suppresses NF-κB p65 and AP-1 transcriptional activation, and restrains reactive astrogliosis[11,12]. Critically, a robust bidirectional crosstalk exists between the TLR4 pathway and BDNF signaling: TLR4 driven neuroinflammation, characterized by elevated TNF-α, IL-1β, and IL-6, directly destabilizes BDNF mRNA via AU rich element (ARE) mediated decay and suppresses BDNF transcription through NF-κB dependent inhibition of CREB activity[13,14]; TLR4 antagonists restore impaired BDNF signaling[15]; and BDNF itself can feedback regulate microglial TLR4 activity and inflammatory responses. Collectively, dysregulation of the TLR4/BDNF signaling axis, characterized by reciprocal suppression between neuroinflammatory activation and neurotrophic support, represents a core pathogenic mechanism driving progressive dopaminergic neurodegeneration in PD.

In recent years, the gut brain axis has emerged as a pivotal pathophysiological framework for understanding the prodromal origins and progressive spread of PD[16]. Accumulating clinical and preclinical evidence demonstrates that PD patients consistently exhibit gut microbiota dysbiosis, characterized by reduced microbial diversity, depletion of short chain fatty acid producing taxa, and enrichment of pro-inflammatory species, as well as increased intestinal permeability, enteric nervous system pathology, and gastrointestinal dysfunction, many of which manifest years prior to the onset of cardinal motor symptoms[17]. Dysregulated gut microbiota and their bioactive metabolites, particularly lipopolysaccharide, short chain fatty acids (SCFAs), and secondary bile acids, modulate central nervous system function via integrated immune, neural, and endocrine pathways[18], for example by promoting the pathological spread of α-syn, exacerbating systemic and brain inflammation[19,20], and downregulating the expression of neurotrophic factors such as BDNF[21,22]. Collectively, these findings position intestinal microenvironment disruption not merely as an early prodromal feature of PD, but as a mechanistically upstream determinant of central neurodegeneration.

Against this backdrop, natural products with multimodal, disease modifying pharmacological profiles, capable of concurrently targeting neuroinflammation, oxidative stress, α-synuclein proteostasis, and neurotrophic signaling, have garnered substantial translational interest. Ginseng (Panax ginseng C.A. Meyer) is a prestigious medicinal and edible homologous plant rich in nutrients, contains bioactive triterpenoid saponins known as ginsenosides (GS), which exhibit robust anti-neuroinflammatory, antioxidant, anti-aggregation, and BDNF enhancing activities in preclinical models of PD[23–25]. Its key component, ginsenoside Re (GsRe), alleviates oxidative stress by activating the Nrf2/GPX4 pathway[26], inhibits the NLRP3 inflammasome[27], and ameliorates neuroinflammation by blocking the AMPKα1/STING signaling pathway[28]. Concurrently, GsRe upregulates the BDNF/TrkB signaling pathway to enhance synaptic plasticity[29], showing protective potential in several in preclinical neurodegenerative

models[30]. Emerging evidence further demonstrates that GS confer neuroprotection, beyond canonical CNS targeted actions, via gut microbiota remodeling. In MPTP induced PD mouse models, GsRe significantly ameliorates motor impairments and preserves nigrostriatal dopaminergic neurons by selectively enriching beneficial commensals and restoring microbial metabolic capacity[31]. Likewise, ginsenoside Rk3 (GsRk3) promotes the expansion of health associated gut microbes and enhances colonic butyrate production, leading to concurrent improvements in locomotor performance and gastrointestinal motility in murine PD models[32].

Accordingly, this study comprehensively investigates the neuroprotective efficacy and multimodal mechanisms of GS and their principal bioactive constituent, GsRe, in the MPTP induced mouse model of PD. GS/GsRe actions across interdependent pathological domains were systematically evaluated: canonical CNS endpoints, including dopaminergic neuron survival, striatal dopamine homeostasis, microglial activation, and synaptic integrity; gut brain axis perturbations, encompassing intestinal barrier dysfunction, enteric glial reactivity, taxonomic and functional shifts in gut microbiota, and host microbe co-metabolite profiles; and the BDNF/TLR4 signaling nexus, specifically testing whether GsRe restores BDNF expression and TrkB signaling while concurrently suppressing TLR4 driven NF-κB activation and downstream pro-inflammatory cytokine production in both gut and brain tissues. By integrating these levels of analysis, a unified mechanistic framework wherein GsRe simultaneously rectifies peripheral dysbiosis and barrier failure was redefined, dampens neuroinflammation via TLR4 inhibition, and rescues neurotrophic support through BDNF upregulation, thereby establishing a rationally grounded, multi-compartment therapeutic paradigm for PD targeting gut brain immune crosstalk.

2. Results

2.1. GS Restores Intestinal Homeostasis and Striatal BDNF/TrkB Signaling in MPTP Induced PD Mice

To elucidate the gut brain axis mediated mechanisms underlying GS efficacy in PD, integrated histological, microbial, metabolomic, and neurotrophic analyses were performed. Intestinal pathology and barrier integrity were evaluated: MPTP triggered mucosal atrophy, crypt distortion, and marked downregulation of OCCLUDIN and ZO-1, effects that were significantly mitigated by GS treatment **(**Fig. 1a**)**. Gut microbiota profiling revealed that MPTP disrupted community structure at both phylum and genus levels **(**Fig. 1b and 1c**)**. At the phylum level, murine gut microbiota exhibited a significant expansion of Firmicutes and a concomitant depletion of Bacteroidota, leading to a markedly decreased Bacteroidota to Firmicutes (B/F) ratio, a microbial signature consistently associated with dysbiosis and metabolic dysfunction. At the genus level, Dubosiella abundance was significantly elevated, with levels exceeding two standard deviations above the healthy control mean, indicating pathological overgrowth rather than physiological fluctuation. GS administration restored taxonomic composition and normalized alpha diversity **(Supplementary Fig. 1a)**. Multivariate ordination (PCA) confirmed clear separation between Vehicle and MPTP groups, with GS treated cohorts clustering closer to Vehicle controls

(Supplementary Fig. 1b), and LefSe analysis identified signature taxa differentially enriched across groups **(Supplementary Fig. 1c)**.

Gut microbiota dysbiosis disrupts BDNF/TrkB signaling axis in both peripheral tissues and the central nervous system, as evidenced by reduced BDNF protein levels. striatal neurotrophic support was assessed: MPTP suppressed BDNF and TrkB protein expression, whereas GS dose dependently reversed this deficit **(**Fig. 1d and 1e**)**. Fecal metabolomics, validated by tight QC sample clustering in both positive and negative ion modes **(Supplementary Fig. 2a and 2b)** and stable TIC profiles **(Supplementary Fig. 2c and 2d)**, identified distinct metabolic signatures: MPTP induced broad perturbations in amino acid, lipid, and neurotransmitter related metabolites, many of which were rescued by GS **(**Fig. 1f and 1g**)**. Supervised OPLS-DA modeling robustly discriminated group differences (Vehicle vs. MPTP; MPTP vs. GS), with permutation tests confirming statistical validity **(**Fig. 1h–1k**)**. Pathway enrichment analysis mapped these metabolic shifts to PD relevant biological processes, including neuroactive ligand receptor interaction and inflammatory mediator regulation of TRP channels, thereby linking systemic metabolic perturbations to established PD pathomechanism. Notably, GS specifically reversed MPTP induced dysregulation in pathways critically governing neuronal survival and synaptic integrity, such as the Toll-like receptor signaling pathway and the neurotrophin signaling pathway, as confirmed by integrated transcriptomic and phosphoproteomic profiling **(**Fig. 1l and 1m**)**.

Finally, network pharmacology integrated multi-omics evidence: a high confidence target overlap between GS bioactive compounds and PD associated genes was identified **(Supplementary Fig. 3a)**; chord and KEGG/GO analyses converged on core pathways, including Neurotrophin, TLR, NF-κB and dopaminergic signaling, implicated in neuroprotection, synaptic plasticity, and inflammation modulation **(Supplementary Fig. 3b–3d)**. Collectively, these findings establish that GS exerts multi-level protection along the gut brain axis, preserving intestinal integrity, reshaping microbiota metabolite crosstalk, and reinforcing striatal neurotrophic resilience in PD.

2.2. GS Attenuates MPTP Induced Motor Deficits and Nigrostriatal Neurodegeneration in PD Mice

To determine the therapeutic impact of GS on PD related behavioral and neuropathological phenotypes, a comprehensive assessment was performed, preceded by rigorous chemical characterization of the GS extract. The experimental timeline and group allocation were defined according to a standardized MPTP intoxication protocol **(**Fig. 2a**)**. GS treatment significantly prevented MPTP induced body weight loss **(**Fig. 2b**)**, rescued spatial learning and memory impairments (reduced total swimming distance and shortened escape latency in the Morris water maze; Fig. 2c and 2d), improved sensorimotor coordination (decreased pole descent latency; Fig. 2e), and enhanced neuromuscular endurance (increased hanging wire test scores; Fig. 2f).

Neuropathological analysis confirmed that GS conferred robust protection against MPTP driven neurodegeneration: striatal neuronal integrity was preserved, as evidenced by restored Nissl positive area coverage **(**Fig. 2g and 2h**)**; dopaminergic neuron survival in the SNpc was markedly improved,

reflected by increased TH immunoreactive neuron counts (Fig. 2i and 2j); and GS normalized the expression of key dopaminergic markers, suppressing pathological α-syn accumulation while restoring TH and DAT protein levels in the striatum (Fig. 2k–2m).

Chemical profiling of GS was conducted using validated UPLC-MS/MS methods: dopamine (DA), 3,4-dihydroxybenzoic acid (DHBA), ginsenoside Re (GsRe), and ginsenoside Rc (GsRc) were unambiguously identified and quantified via selective reaction monitoring (SRM) transitions **(Supplementary Fig. 4a–4d)**; the chromatographic resolution and overall metabolic profile of the GS extract were confirmed by total ion current (TIC) analysis **(Supplementary Fig. 4e)**; and the structural authenticity of GsRe was further verified by UPLC-MS/MS fragmentation patterns **(Supplementary Fig. 4f)**.

Together, these data establish that GS exerts functional and structural neuroprotection in MPTP induced PD, with its bioactive composition rigorously authenticated to underpin mechanistic interpretation.

2.3. GS Suppresses MPTP Induced Neuroinflammation, Neuronal Apoptosis, and TLR4/NF-κB Activation in PD Mice

To elucidate the molecular mechanisms underlying GS mediated neuroprotection, targeted assessments of neuroinflammatory status, NF-κB signaling dynamics, and apoptotic execution were performed. ELISA quantification revealed that MPTP significantly elevated pro-inflammatory cytokines TNF-α and IL-1β while suppressing anti-inflammatory mediators TGF-β and IL-10 in brain tissue, effects fully normalized by GS treatment (Fig. 3a–3d). IF confirmed that MPTP triggered robust nuclear translocation of NF-κB, a hallmark of canonical inflammatory activation, which was potently inhibited by GS (Fig. 3e).

Western blot analysis demonstrated that MPTP upregulated TLR4 expression and induced phosphorylation of NF-κB at Ser529, indicative of pathway activation, both of which were significantly attenuated by GS (Fig. 3f and 3g). Similarly, MPTP shifted the Bcl-2/Bax ratio toward apoptosis and increased cleaved caspase-3 levels; GS restored the anti-apoptotic balance and suppressed caspase-3 cleavage (Fig. 3h and 3i). These findings collectively establish that GS confers neuroprotection by concurrently dampening neuroinflammatory responses, inhibiting TLR4/NF-κB signaling, and blocking intrinsic apoptotic cascades.

2.4. BDNF Deficiency Exacerbates MPTP Induced Nigrostriatal Degeneration, Motor Deficits, and Neuroinflammation in PD Mice

To determine the functional contribution of endogenous BDNF to PD resilience, parallel phenotypic assessments were performed in BDNF cKO and WT mice subjected to MPTP intoxication. First, the BDNF cKO model was validated: genotype identification via gel electrophoresis confirmed expected band sizes for WT, heterozygous (Het), and cKO mice **(Supplementary Fig. 5c)**, and BDNF protein levels were confirmed to be significantly reduced in cKO mice relative to controls **(Supplementary Fig. 5b)**.

Immunohistochemical analysis revealed that BDNF cKO significantly intensified MPTP induced loss of TH immunoreactive neurons in the SNpc **(**Fig. 4a and 4b**)**. Consistent with this, BDNF cKO amplified MPTP driven α-syn accumulation and TH depletion in the striatum and midbrain, as confirmed by Western blotting **(**Fig. 4c and 4d**)**, and further reduced striatal dopamine (DA) levels beyond those observed in MPTP treated WT controls **(**Fig. 4e**)**. Motor performance was markedly worsened by BDNF cKO: both hanging wire endurance **(**Fig. 4f**)** and pole descent latency **(**Fig. 4g**)** showed greater impairment in BDNF cKO MPTP mice relative to MPTP treated WT mice, with spatial exploration patterns in the Morris water maze (MWM) test, visualized via heatmap, reflecting more disorganized trajectories in BDNF cKO mice **(Supplementary Fig. 5a)**.

Moreover, BDNF cKO potentiated MPTP induced neuroinflammation, as evidenced by significantly higher levels of tumor necrosis factor-α (TNF-α) and interleukin-1β (IL-1β) in brain homogenates **(**Fig. 4h and 4i**)**. To extend these findings to human PD, bioinformatic analysis of the GSE49036 dataset was conducted: a volcano plot highlighted that BDNF expression was significantly downregulated in PD patients relative to healthy controls **(Supplementary Fig. 5d)**.

These data demonstrate that endogenous BDNF constrains multiple facets of PD pathogenesis, including dopaminergic neuron vulnerability, behavioral dysfunction, and inflammatory activation, thereby establishing BDNF as a key endogenous modulator of disease progression, with relevance to both preclinical models and human PD.

2.5. GsRe, a Principal GS Bioactive Constituent, Engages BDNF, Crosses the BBB, and Rescues Dopaminergic Dysfunction in PD Models

To identify bioactive components of GS responsible for its neuroprotective effects, molecular docking and cell-based screening were conducted. First, saponin compounds in ginseng were comprehensively identified using ultra-high performance liquid chromatography (UHPLC) coupled with Q-Orbitrap tandem mass spectrometry (UHPLC-Q-Orbitrap MS/MS), and their chemical structures were unambiguously elucidated based on high resolution MS data, characteristic fragmentation patterns, and comparison with reference standards or literature **(Table)**. In addition, molecular docking analyses of major GS components with BDNF were performed; among them, GsRc (binding energy: -8.1 kcal/mol), GsRg2 (-7.3 kcal/mol), GsRb2 (-7.8 kcal/mol), and GsRe (-7.4 kcal/mol) showed high binding affinity to BDNF **(Supplementary Fig. 6a–6h)**.

Subsequently, cell-based screening was carried out to evaluate the protective effects of these components against MPP^+ induced cytotoxicity in SH-SY5Y cells. A dose response curve confirmed MPP^+ induced cytotoxicity in SH-SY5Y cells **(Supplementary Fig. 7a)**, and no significant cytotoxicity was observed for GS or its monomeric saponins (GsRe, GsRg2, GsRb2, GsRc, GsRo) at tested concentrations **(Supplementary Fig. 7b–7g)**. Pretreatment with GS, GsRe, GsRg2, GsRb2, or GsRc significantly reversed MPP^+ induced cell viability reduction, with GsRe showing robust protective activity **(Supplementary Fig. 7h–7m)**.

To validate GsRe's in vivo activity, its BBB permeability and regulatory effects on BDNF/DA signaling were assessed. Molecular docking confirmed GsRe's binding to BDNF with a binding energy of -7.4 kcal/mol (Fig. 5a). CCK-8 assay further verified GsRe's protective effect against MPP^+ induced neuronal cell viability loss (Fig. 5b). Western blot analyses showed that GsRe upregulated BDNF and its receptor TrkB protein expression (Fig. 5c and 5d). UPLC-MS/MS quantification revealed that GsRe increased DA content in serum, striatum, and SNpc (Fig. 5e and 5g), and was detected in serum, striatum, and SNpc, confirming its ability to cross the BBB (Fig. 5h–5j).

Collectively, these data establish GsRe not merely as a high affinity BDNF ligand, but as a BBB permeable, multi-target neuroprotectant that mechanistically links BDNF signaling restoration to dopaminergic rescue in PD.

2.6. GsRe Rescues Motor Dysfunction and Dopaminergic Degeneration in PD Mouse Models

To determine whether GsRe mediated BDNF/DA pathway modulation translates into functional recovery, comprehensive behavioral phenotyping was performed. GsRe treatment significantly restored spontaneous locomotor activity, as reflected by increased total distance traveled in the open field test (Fig. 6a), and normalized gait parameters, including stride length (Fig. 6b). Furthermore, GsRe improved dynamic motor coordination, evidenced by reduced pole descent latency (Fig. 6c) and enhanced neuromuscular endurance on the hanging wire test (Fig. 6d), indicating rescue of both axial and limb motor control.

At the neuroanatomical level, GsRe attenuated MPTP induced degeneration of TH immunoreactive neurons in the SNpc (Fig. 6e and 6f) and preserved dopaminergic terminal density in the striatum, as confirmed by dual IF staining for TH and DAT (Fig. 6g-6k). Consistent with these morphological improvements, GsRe suppressed pathological α-syn accumulation and restored expression levels of TH and DAT proteins in the midbrain striatal circuit (Fig. 6l–6n). Critically, these protective effects were retained in BDNF cKO mice subjected to MPTP, where GsRe significantly ameliorated motor deficits and neuronal loss relative to the BDNF cKO + MPTP group, demonstrating its capacity to functionally compensate for endogenous BDNF deficiency.

Collectively, these findings establish GsRe as a disease modifying agent that restores motor behavior and halts dopaminergic degeneration across distinct PD etiologies, including BDNF deficient states, thereby supporting its translational potential for heterogeneous PD populations.

2.7. GsRe Attenuates BDNF Deficiency Exacerbated TLR Signaling Activation via Proteomic and Molecular Validation

To elucidate how GsRe rescues dopaminergic deficits in BDNF deficient PD models, integrated proteomic and mechanistic validation was performed. Venn analysis identified a core set of overlapping

differentially expressed proteins (DEPs) shared between BDNF cKO + MPTP vs. WT + MPTP and BDNF cKO + MPTP vs. BDNF cKO + GsRe comparison enriched in TLR signaling components (Fig. 7a). Consistent with this, KEGG enrichment revealed robust activation of the TLR pathway in BDNF cKO + MPTP mice relative to WT + MPTP controls (Fig. 7b), whereas GsRe treatment reversed this signature, significantly enriching for TLR signaling suppression and neuroprotective pathways (Fig. 7c).

GsRe administration markedly suppressed expression of canonical TLR4 pathway effectors, including TLR4, TRIF, NF-κB, and p-NF-κB, in the midbrain of BDNF cKO + MPTP mice (Fig. 7d–7e). Crucially, molecular docking predicted high affinity binding between BDNF and TLR4 (− 20.5 kcal/mol; Fig. 7f), which was experimentally confirmed by Co-IP (Fig. 7g). Volcano plot analysis further corroborated pathway level modulation, showing coordinated downregulation of pro-inflammatory DEPs and upregulation of regulatory factors (Fig. 7h). Notably, GsRe restored WDFY1 and suppressed STAT1, reinforcing its dual inhibitory action on upstream receptor engagement and downstream effector activation (Fig. 7i and 7j).

Complementary quality control analyses confirmed behavioral fidelity and proteomic robustness: OFT trajectory heatmaps and footprint gait patterns demonstrated reproducible motor phenotypes across groups **(Supplementary Fig. 8a and 8b)**; PCA and hierarchical clustering showed tight intra group clustering and clear inter group separation **(Supplementary Fig. 8c and 8d)**; and DEP overlap heatmaps, together with GO enrichment, consistently linked BDNF deficiency to PD relevant pathogenic processes **(Supplementary Fig. 8e and 8f)** and GsRe to anti-inflammatory, neurotrophic, and synaptic resilience pathways **(Supplementary Fig. 8g)**.

Together, these data establish that GsRe counteracts BDNF deficiency aggravated neuroinflammation by directly disrupting the BDNF/TLR4 interaction and rebalancing TLR4/NF-κB/STAT1 axis activity, thereby providing a unified mechanistic explanation for its concurrent rescue of motor dysfunction, dopaminergic integrity, and gut brain axis homeostasis observed across multiple experimental paradigms.

2.8. GsRe Suppresses TLR4 Driven Neuroinflammation, M1 Microglial Polarization, and Caspase-3 Dependent Apoptosis in BDNF Deficient PD Mice

To determine whether GsRe counteracts TLR4 dependent neuroimmune dysregulation in BDNF deficient PD models, microglial phenotype, cytokine balance, and apoptotic signaling were systematically assessed. GsRe treatment significantly reduced Iba-1$^+$/CD86$^+$ (M1) microglia and increased Iba-1$^+$/CD206$^+$ (M2) microglia, evidencing a functional shift from pro-inflammatory to reparative microglial states (Fig. 8a). Consistently, GsRe lowered Iba-1 MFI (Fig. 8b) and markedly decreased the CD86/CD206 MFI ratio (Fig. 8c), confirming suppression of M1 polarization at both cellular and molecular levels.

GsRe robustly suppressed pro-inflammatory mediators TNF-α and IL-1β (Fig. 8d–8e), while concurrently elevating anti-inflammatory cytokines TGF-β and IL-10 (Fig. 8f and 8g), demonstrating bidirectional

immunomodulation within the neuroinflammatory milieu. At the execution level of neuronal death, GsRe increased Bcl-2 expression, decreased Bax, and abolished cleaved caspase-3 accumulation (Fig. 8h and 8i), indicating potent inhibition of the intrinsic mitochondrial caspase apoptotic cascade. Together, these findings establish that GsRe disrupts the TLR4 microglial M1/cytokine/apoptosis axis in BDNF deficient PD mice, providing mechanistic convergence across neuroinflammation, immune cell reprogramming, and neuronal survival endpoints.

3. Discussion

This study provides compelling evidence that GS and their bioactive constituent GsRe confer robust, multi-level neuroprotection in the MPTP induced murine model of PD. Critically, this protection operates through an integrated gut brain axis mechanism, initiating with restoration of intestinal barrier integrity and microbial homeostasis, and culminating in central modulation of the BDNF/TLR4 signaling nexus. Behavioral assessments and neuropathological analyses consistently demonstrate that GS and GsRe significantly attenuate motor deficits and preserve tyrosine hydroxylase positive dopaminergic neurons in the SNpc. Mechanistically, GS ameliorates MPTP triggered colonic epithelial damage, dysbiosis of the gut microbiota, and associated perturbations in host metabolite profiles. Notably, GsRe is confirmed to cross the BBB, elevate endogenous BDNF expression in the striatum and midbrain, and thereby suppress hyperactivation of the TLR4/NF-κB cascade. Quantitative proteomics further corroborates that GsRe driven neuroprotection is functionally linked to coordinated regulation of BDNF dependent TLR signaling components. Specifically, enhanced BDNF signaling inhibits excessive TLR4 mediated NF-κB nuclear translocation, leading to reduced microglial polarization toward the pro-inflammatory M1 state, diminished secretion of TNF-α, IL-1β, and other inflammatory mediators, and consequent attenuation of caspase dependent neuronal apoptosis.

Growing experimental and clinical evidence indicates that gut microbiota dysbiosis and intestinal barrier dysfunction are not merely secondary consequences but represent early, pathogenic events that actively contribute to PD initiation and progression[33]. In this study, MPTP administration triggered concurrent central and enteric pathology: it induced progressive dopaminergic neurodegeneration in the SNpc while simultaneously eliciting marked intestinal epithelial damage, profound gut microbiota dysbiosis, and significant alterations in the fecal metabolome. Notably, PD mice exhibited a pronounced reduction in the Bacteroidota to Firmicutes ratio shift consistently associated with impaired gut barrier function and systemic inflammation. Bacteroidota species are key contributors to the microbial fermentation of dietary fiber into SCFAs, particularly butyrate[34], which exerts neuroprotective effects by reinforcing intestinal barrier integrity, modulating microglial activation, and supporting dopaminergic neuron survival through HDAC inhibition and BDNF upregulation[35]. GS treatment robustly restored intestinal homeostasis, reversing epithelial damage, normalizing microbial community structure, and rescuing fecal metabolite profiles, thereby functionally reconstructing the gut brain axis. This aligns with emerging evidence demonstrating that ginsenosides exert disease modifying effects in PD not merely through

direct neuronal actions, but primarily by remodeling the gut microbiota and its functional output, culminating in a coordinated microbiota/metabolite/ neuroprotection axis[31,32,36].

Integrated metabolomic profiling and network pharmacology guided KEGG pathway enrichment analysis revealed that GS intervention significantly modulates metabolic pathways, particularly those linked to neurotrophic signaling and innate immune activation, indicating a systems level coordination between peripheral metabolism and central nervous system homeostasis. Accumulating evidence demonstrates that gut microbiota composition exerts robust regulatory control over cerebral BDNF expression[37]. Specifically, the relative abundance of beneficial commensals, including ‘Muribaculum’, shows a strong positive correlation with striatal BDNF protein levels[38], whereas ‘Allobaculum’ abundance inversely correlates with BDNF expression[39]. Conversely, clinical studies report elevated TLR4 expression in the colonic mucosa of PD patients, which significantly associates with increased luminal and systemic concentrations of pro-inflammatory cytokines such as TNF-α and IL-6[40]. In preclinical models, fecal microbiota transplantation (FMT) from PD donors recapitulates key neuropathological features, including α-syn aggregation in the enteric and central nervous systems and progressive motor deficits, effects that are mechanistically dependent on TLR4 signaling activation[41]. These findings collectively support the hypothesis that maladjusted gut microbial configurations serve as critical environmental drivers of chronic, low grade TLR4 pathway activation. Consistent with this, a marked expansion of ‘Dubosiella’ was observed in the cecum and colon of MPTP induced PD mice[42], a genus previously implicated in both modulation of BDNF biosynthesis and potentiation of TLR4 dependent inflammatory responses via secretion of immunomodulatory metabolites[43,44]. Critically, GS treatment normalized ‘Dubosiella’ abundance, restored host metabolic homeostasis, suppressed intestinal and systemic pro-inflammatory mediators, and enhanced BDNF synthesis in both gut and brain tissues, thereby establishing a peripherally initiated, metabolically reinforced anti-inflammatory and neurotrophic milieu conducive to CNS protection.

Within the innate immune system, TLR4 serves as a pivotal pattern recognition receptor that initiates and amplifies neuroinflammatory signaling cascades, thereby directly contributing to neuronal dysfunction, microglial hyperactivation, and progressive neurodegeneration in PD and other CNS disorders[45,46]. TLR4 expression is significantly elevated in PBMCs isolated from PD patients, and this upregulation shows a robust positive correlation with circulating concentrations of TNF-α, a key pro-inflammatory cytokine implicated in dopaminergic neurodegeneration[47]. During PD pathogenesis, misfolded α-syn undergoes progressive conformational transition into neurotoxic oligomers and insoluble fibrillar aggregates, both of which function as endogenous danger associated molecular patterns (DAMPs) capable of direct recognition by TLR4 expressed on microglia and neurons, thereby triggering canonical innate immune signaling and sustained neuroinflammatory responses[48]. Upon activation of microglial TLR4, NF-κB signaling is induced through MyD88- or TRIF dependent pathways[49]. NF-κB activation exerts dual inhibitory effects on major intracellular protein degradation pathways, specifically suppressing both autophagic flux and ubiquitin proteasome system (UPS) activity, thereby compromising the cellular

capacity to clear misfolded α-syn, promoting its accumulation into toxic oligomers and aggregates, and ultimately accelerating neurodegeneration[50]. Furthermore, NF-κB drives microglial polarization toward the pro-inflammatory M1 phenotype, promoting the release of inflammatory mediators such as TNF-α and IL-1β[51]. These inflammatory mediators exert direct neurotoxic effects on dopaminergic neurons while concurrently inducing oxidative stress and impairing mitochondrial bioenergetics, including reduced ATP production, increased ROS generation, and loss of mitochondrial membrane potential, thereby triggering intrinsic apoptotic signaling through caspase-9 and caspase-3 activation and culminating in irreversible neuronal apoptosis[52].

BDNF, the central focus of this study, exerts a dual, functionally opposing role in PD pathogenesis: it serves as both a critical neurotrophic mediator essential for dopaminergic neuron survival, synaptic maintenance, and functional integrity, and a potent endogenous suppressor of neuroinflammatory signaling[53]. Findings demonstrate that BDNF deficiency markedly exacerbates MPTP induced neuropathology, as evidenced by elevated α-syn accumulation, diminished TH expression in the SNpc, reduced striatal dopamine content, and pronounced motor deficits. These observations align with prior preclinical and clinical evidence[54], and mechanistic studies suggest that BDNF loss may impair presynaptic dopamine reuptake efficiency and downregulate glutamate decarboxylase 65/67 (GAD65/67) expression, thereby disrupting dopaminergic and GABAergic circuit balance[55–57]. Concurrently, BDNF deficiency amplifies neuroinflammatory responses through multiple non-redundant mechanisms: it attenuates inhibition of NF-κB nuclear translocation, leading to enhanced transcription of pro-inflammatory mediators[58]; in LPS challenged models, exogenous BDNF administration significantly suppresses microglial activation markers, including Iba1, CD68, and MHC-II, and dampens cytokine release[59]; and clinically, cerebrospinal fluid (CSF) BDNF levels in PD patients show a robust inverse correlation with CSF concentrations of TNF-α, IL-1β, and IL-6[60]. Collectively, these data position BDNF as a pivotal node integrating neurotrophic support and immune homeostasis in PD.

Proteomic profiling identified BDNF deficiency as a critical upstream driver of pathological TLR4 pathway hyperactivation in preclinical PD models. This observation is corroborated by convergent evidence across diverse experimental systems: in enteric glial cells, BDNF has been shown to directly suppress intestinal TLR4 signaling[61]; in oxygen glucose deprivation models, pharmacological or genetic activation of the BDNF/TrkB axis significantly downregulates microglial TLR4 expression[62]. Collectively, these findings indicate that physiological BDNF signaling imposes tonic inhibition on the TLR4 pathway, and its loss removes this regulatory constraint. Consistent with this model, conditional BDNF knockout in a PD context led to marked upregulation of WDFY1, a selective autophagy adaptor protein integral to endosomal TLR3/TLR4 signaling[63]. WDFY1 facilitates TRIF recruitment and robustly amplifies downstream NF-κB and IRF3 activation, thereby enhancing transcription of pro-inflammatory cytokines including TNF-α, IL-6, and type I interferons[64,65]. Thus, BDNF deficiency disrupts homeostatic suppression of WDFY1, resulting in unchecked TLR4/TRIF/NF-κB/IRF3 signaling, sustained microglial pro-inflammatory polarization, and progressive neuroinflammation, a core pathogenic axis in PD.

Notably, elevated WDFY1 expression has also been documented in postmortem brain tissue from individuals with schizophrenia[66], suggesting that dysregulation of the BDNF/WDFY1/TLR4 axis may represent a shared molecular mechanism across multiple neuropsychiatric disorders. Critically, GsRe exerts its anti-neuroinflammatory effect by restoring physiological BDNF levels, thereby reinstating negative regulation over this cascade and attenuating downstream inflammatory pathology.

Several limitations warrant careful consideration. First, while this study rigorously establishes BDNF mediated suppression of the TLR4/NF-κB inflammatory axis as a central mechanism of GsRe action, it does not comprehensively assess concurrent modulation of the canonical TrkB dependent neurotrophic pathway. Given that BDNF/TrkB signaling is essential for neuronal survival, synaptic plasticity, and anti-apoptotic function, its attenuation under pathological conditions, such as MPTP induced BDNF deficiency, may create a permissive cellular milieu that indirectly favors unchecked TLR4 activation and pro-inflammatory polarization. Second, although GsRe treatment robustly normalized dysregulated TLR4 expression and downstream NF-κB activity in PD mice, the potential contribution of TrkB pathway engagement, and its functional crosstalk with inflammatory cascades, remains to be experimentally validated. Future studies employing TrkB specific inhibitors or conditional TrkB knockout models will be critical to dissect whether GsRe`s anti-inflammatory efficacy is, at least in part, contingent upon TrkB activation and subsequent pathway integration.

In summary, this study comprehensively delineates a unified gut brain mechanism through which GS and their principal bioactive constituent GsRe confer neuroprotection in PD. GS and GsRe act synergistically across anatomical compartments: they restore intestinal barrier function and microbial ecology while concurrently enhancing central BDNF signaling, leading to downstream suppression of TLR4/NF-κB driven neuroinflammation, attenuation of dopaminergic neuron loss in the SNpc, and significant improvement in motor performance. Collectively, these results establish a mechanistically grounded framework for gut brain targeted interventions and offer robust preclinical evidence supporting the development of multi-target therapeutic approaches for PD.

4. Materials and Methods

4.1. Chemical Reagents

GS were procured from Shanghai Yuan Ye Biotechnology Co., Ltd. (Shanghai, China; lot: J03GS153706). Individual ginsenoside standards, including Rg1 (C42H72O14; lot: JB263899), Re (C48H82O18; lot: O21IS229576), Rb1 (C54H92O23; lot: N18GB163839), Rd (C48H82O18; lot: JB238591), Rf (C42H72O14; lot: P25F12L140073), Rg2 (C42H72O13; lot: JB266498), Rc (C53H90O22; lot: N27HB202514), and Ro (C48H76O19; lot: A02IB211532), were likewise supplied by the same vendor. High performance liquid chromatography (HPLC) grade acetonitrile and methanol were obtained from Fisher Scientific (Pittsburgh, PA, USA). Carbidopa/levodopa sustained-release tablets (50 mg/200 mg per tablet) were sourced from Merck Sharp & Dohme (Hangzhou MSD Pharmaceutical Co., Ltd., Hangzhou, China).

4.2. The Chemical Constituents of GS Were Isolated and Characterized via UHPLC Coupled with Q-Orbitrap Tandem Mass Spectrometry

Qualitative profiling of GS was conducted using ultra-high-performance liquid chromatography coupled with Q-Orbitrap tandem mass spectrometry (UHPLC-Q-Orbitrap-MS/MS). Briefly, 30.0 mg of finely ground GS sample was accurately weighed and extracted with 10.0 mL of 70% (v/v) methanol under ultrasonic assistance for complete solubilization. The resulting extract was filtered through a 0.22 μm polytetrafluoroethylene (PTFE) membrane before analysis. Chromatographic separation was performed on a Waters ACQUITY UPLC BEH C18 column (2.1 mm × 100 mm, 1.7 μm particle size) maintained at 35°C. The mobile phase comprised solvent A (0.1% formic acid in water) and solvent B (acetonitrile), delivered at a constant flow rate of 0.3 mL/min. A 2 μL aliquot was injected per run. Gradient elution was programmed as follows: 0–12 min, 82–80% A; 12–14 min, 80–70% A; 14–24 min, 70–68% A; 24–29 min, 68–67% A; 29–49 min, 67–25% A; 49–55 min, 25–0% A (i.e., 0–82% B); 55–60 min, isocratic at 0% A (82% B). Mass detection was carried out in negative electrospray ionization (ESI^-) mode. Key MS parameters included: sheath gas flow, 35 arbitrary units (Arb); auxiliary gas flow, 10 Arb; sweep gas flow, 1 Arb; S-lens RF level, 55%; capillary voltage, − 3.5 kV; capillary temperature, 350°C. Full-scan MS spectra were acquired over m/z 150–2000 at a resolution of 70,000 (at m/z 200), with an AGC target of 3×10^6 and a maximum injection time of 100 ms. For data-dependent MS/MS acquisition, the resolution was set to 17,500 (at m/z 200), AGC target to 1×10^5, injection time to 50 ms, top five precursors selected per cycle, isolation window of 4.0 *m/z*, and normalized collision energy stepped across 25, 35, and 55 eV.

4.3. PCR and 16S rRNA Sequencing

Following the final dosing, mice were subjected to a 12-hour fasting period prior to collection of freshly voided fecal samples. Total genomic DNA was isolated from fecal material using the OMEGA Soil DNA Kit (Cat. No. MS635-02; Omega Bio-Tek, Norcross, GA, USA), according to the manufacturer's instructions. The hypervariable V3–V4 region of the bacterial 16S rRNA gene was amplified via PCR using the forward primer ACTCCTACGGGAGGCAGCA and reverse primer GGACTACHVGGGTWTCTAAT. Purified amplicons were sequenced on an Illumina HiSeq platform. Library preparation, high throughput sequencing, and subsequent bioinformatic processing, including quality filtering, operational taxonomic unit (OTU) clustering, and taxonomic assignment, were performed by Shanghai Personal Biotechnology Co., Ltd.

4.4. Metabolomic Analyses

Approximately 20 mg of fresh fecal material was accurately weighed and transferred to a 2 mL centrifuge tube pre-chilled on ice. To each sample, 300 μL of ice-cold methanol containing 5 ppm 2-chlorophenylalanine (as an internal standard) was added, along with two stainless steel beads. The mixture was vortexed vigorously for 30 seconds, followed by mechanical homogenization at 55 Hz for 60 seconds using a tissue lyser. Subsequently, the suspension was subjected to ultrasonication in an ice-water bath for 10 minutes, then incubated at − 20°C for 30 minutes to precipitate proteins. After centrifugation at 12,000 × g and 4°C for 10 minutes, the clear supernatant was carefully collected,

filtered through a 0.22 μm PTFE membrane, and transferred into a chilled autosampler vial. Chromatographic separation was performed on an ACQUITY UPLC HSS T3 column (2.1 mm × 100 mm, 1.8 μm, 100 Å pore size) maintained at 40°C. The autosampler tray temperature was set to 8°C, and a 2 μL injection volume was used. Mobile phases consisted of solvent A: 0.1% (v/v) formic acid in water; solvent B: acetonitrile containing 0.1% (v/v) formic acid. Gradient elution was applied as follows: 0–1 min, 5% B; 1–4.7 min, linear increase from 5% to 95% B; 4.7–6 min, isocratic at 95% B; 6–6.1 min, rapid re-equilibration to 5% B; 6.1–8.5 min, isocratic hold at 5% B.

4.5. Quantitative Determination of GsRe and Dopamine

Metabolite quantification was conducted using Waters Xevo TQ-XS triple quadrupole mass spectrometer coupled with UHPLC. For serum analysis, 100 μL of each sample was processed; for tissue samples, homogenization was performed in ice-cold normal saline at a ratio of 1:5 (w/v), and the supernatant obtained after centrifugation was used, 100 μL per sample. To ensure analytical precision, 20 μL of either 2,3-dihydroxybenzoic acid (DHBA) or ginsenoside Rc (GsRc) solution was spiked as an internal standard. Proteins were precipitated by adding acetonitrile containing 0.1% formic acid. Following centrifugation, the organic layer was carefully transferred and dried under a gentle stream of nitrogen. The residue was reconstituted in 20 μL of a methanol water mixture (8:2, v/v) containing 0.2% formic acid prior to injection. Chromatographic separation was achieved on an ACQUITY UPLC® BEH C18 column (2.1 mm × 50 mm, 1.7 μm) maintained at ambient temperature. Mobile phases consisted of solvent A (acetonitrile) and solvent B (0.1% formic acid in water). Dopamine (DA) was detected in electrospray positive ion mode (ESI^+) using the following gradient: 0–2.5 min, 5% A; 2.5–4 min, linear ramp to 20% A; 4–7 min, further increase to 60% A; 7–7.5 min, rapid return to 5% A; 7.5–10 min, isocratic hold at 5% A. A 3 μL injection volume and a flow rate of 0.2 mL/min were employed. In contrast, GsRe was monitored in ESI^- mode with a distinct gradient: 0–9 min, linear increase from 12% to 90% A; 9–12 min, immediate re-equilibration to 12% A. For this analysis, the injection volume remained 3 μL, while the flow rate was increased to 0.4 mL/min.

4.6. Network Pharmacology

The canonical SMILES strings of GS and its bile acid derived metabolites were retrieved from PubChem and submitted to the SwissTargetPrediction platform to infer putative molecular targets. Concurrently, PD associated genes were systematically compiled from three authoritative resources: OMIM, DisGeNET, and GeneCards. Overlapping targets shared across all three databases were identified using Venn diagram intersection analysis. These consensus targets were then uploaded to the STRING database (version 11.5) to generate a high confidence protein–protein interaction (PPI) network, with interaction scores set above the medium confidence threshold (combined score > 0.4). Subsequently, functional enrichment analyses, including biological process, molecular function, and cellular component terms under Gene Ontology (GO), as well as pathway level insights from the Kyoto Encyclopedia of Genes and Genomes (KEGG), were conducted using the DAVID Bioinformatics Resources (v6.8), applying Benjamini Hochberg correction for multiple testing (adjusted $p < 0.05$ considered significant).

4.7. Molecular Docking

The high-resolution X ray crystal structure of BDNF, deposited in the Protein Data Bank under accession code 1BND, was downloaded and prepared for docking studies. Three-dimensional structural coordinates of ginsenoside derived bioactive compounds were acquired from the Traditional Chinese Medicine Systems Pharmacology (TCMSP) database. Using PyMOL (v2.5), the BDNF structure was preprocessed by removing co-crystallized ligands, nonessential water molecules, and heteroatoms; hydrogen atoms were then added, atomic charges assigned via the AMBER ff14SB force field, and the protein was designated as the receptor molecule. All atoms were optimized and saved in PDBQT format, a prerequisite for AutoDock Vina. Molecular docking simulations were carried out using AutoDock Vina 2.1.6 with a grid box centered on the functionally relevant dimer interface region (size: 30 × 30 × 30 $Å^3$, spacing: 0.375 Å). For each ligand, 20 independent docking runs were performed, and the top-scoring pose, defined by the lowest predicted binding energy and supported by consistent clustering across multiple runs, was selected as the representative binding conformation. Final structural analysis, including interaction mapping, hydrogen bond detection, hydrophobic contact visualization, and surface representation, was conducted using PyMOL 3.1 and Discovery Studio 2019 (Biovia).

A computational rigid-body docking analysis was performed to predict the binding mode between BDNF (UniProt accession P21237) and TLR4 (UniProt accession Q9QUK6), employing the GRAMM-X online platform. The three-dimensional coordinates of both proteins were obtained from UniProtKB in PDB format; regions with incomplete atomic detail were reconstructed via homology modeling using MODELLER, followed by rigorous stereochemical validation. All docking runs adhered to GRAMM-X's built-in default configuration. Compassing standard grid spacing, the integrated scoring algorithm, and default conformational search settings. From the ensemble of predicted poses, the highest scoring complex, prioritized according to geometric fit and interfacial energetics, was further analyzed using PDBePISA to compute estimated binding free energy and dissect physicochemical features of the protein–protein interface (PPI). Visualization and structural characterization, including molecular surface rendering, identification of contact residues at the binding site, and generation of 2D interaction schematics, were carried out using PyMOL version 3.1.

4.8. Animals

Male mice with a conditional deletion of the BDNF gene (BDNF cKO) were generously supplied by Prof. Zheyu Chen's research group, Department of Neurobiology, Shandong University. Age matched wildtype (WT) male C57BL/6 mice (8 weeks old, specific pathogen free grade) were purchased from Liaoning Changsheng Biotechnology Co., Ltd. Animals were housed individually in ventilated cages under controlled environmental conditions: ambient temperature held at 20 ± 2°C, relative humidity maintained at 50 ± 5%, and a fixed 12-hour light, 12-hour dark schedule (light onset at 07:00). Standard rodent diet and sterilized drinking water were provided continuously without restriction. All experimental procedures involving animals conformed strictly to the ethical standards outlined in the 'Guide for the Care and Use

of Laboratory Animals' (National Research Council, 2011) and received prior authorization from the Institutional Animal Care and Use Committee (IACUC) of Changchun University of Chinese Medicine.

4.9. Cell Cultivation

Human neuroblastoma SH-SY5Y cells were acquired from Wuhan Zishan Biological Technology Co., Ltd. Cells were cultured in Dulbecco's Modified Eagle Medium (DMEM) supplemented with 10% heat-inactivated fetal bovine serum (FBS), 100 U/mL penicillin, and 100 μg/mL streptomycin, under standard conditions: 37°C in a humidified atmosphere containing 5% CO_2. To model dopaminergic neuronal injury in vitro, cells were pretreated with graded concentrations of GS or individual GSs, including Re, Rf, Rg_2, Rc, and Ro, for 2 hours, followed by co-exposure to 0.5 mM 1-methyl-4-phenylpyridinium iodide (MPP^+; Macklin, Cat. No. C17441450) for an additional 24 hours. Cell viability was quantified using the Cell Counting Kit-8 (CCK-8; BIOSS, Lot No. BE05068677). Briefly, after treatment, 10 μL of CCK-8 reagent was added per well, and plates were incubated at 37°C for 60 minutes in the dark. Absorbance was then measured at 450 nm using a Synergy H1 microplate reader (BioTek), with background subtraction at 630 nm. All assays were performed in triplicate across at least three independent experiments.

4.10. Animal Grouping and Behavior Assessment

Following a 7-day acclimatization period, mice were intraperitoneally injected with MPTP at a dose of 25 mg/kg daily for 7 consecutive days, while the control group received an equivalent volume of normal saline. Successful model establishment was determined based on significant behavioral changes observed after MPTP administration compared to baseline. Successfully modeled wild-type mice were randomly assigned to the following groups: MPTP group, positive control (P.C.) group (Carbidopa and Levodopa Sustained Release Tablets, 50 mg/kg[67]), GS high-, medium-, and low dose groups (100, 50, and 25 mg/kg, respectively), and GsRe group (40 mg/kg). BDNF cKO mice were randomly divided into the MPTP and GsRe (40 mg/kg) groups. All interventions were delivered once daily by oral gavage for a total duration of 21 days. Mice in the control and disease model groups were administered an isovolumetric dose of sterile saline. In the treatment groups, drug administration was weight adjusted; the vehicle control group received saline at a volume corresponding to that used for the 50 mg/kg drug dose.

Pole Test

This behavioral assay is widely used to assess neuromuscular function and motor coordination in rodents. The apparatus consists of a vertical wooden pole (30 cm long, 2 cm in diameter) mounted centrally within a transparent plastic enclosure; its surface is wrapped with two layers of sterile gauze to ensure adequate traction. At the start of each trial, the mouse is gently restrained by the tail and placed head down on the upper end of the pole, allowing its forelimbs to grasp the top. The stopwatch is triggered upon release and stopped when the animal's forepaws first contact the floor of the chamber. To reduce performance variability due to fatigue or learning effects, three trials are conducted per animal, separated by 20-minute rest periods. The mean latency across the three attempts is taken as the representative outcome measure for each subject.

Hanging Rope Test: A horizontal stainless-steel wire (approximately 40 cm long) was suspended 30 cm above a padded surface. Each mouse was carefully positioned at the midpoint of the wire, with its forelimbs gripping the center. Motor function was quantified using a validated three component scoring protocol: (1) Forelimb grip initiation latency: scored from 1 to 5 based on the time required to secure grip ≤ 4 s (5 points), 5–9 s (4 points), 10–19 s (3 points), 20–39 s (2 points), and ≥ 40 s (1 point); (2) Wire traversal time: scored 5–1 for completing movement to either end within ≤ 39 s, 40–59 s, 60–99 s, 100–129 s, or ≥ 130 s, respectively; (3) Fall latency: assigned scores of 5 (no fall during the 180-s observation window), 4 (fall after ≥ 120 s), 3 (60–119 s), 2 (20–59 s), or 1 (< 20 s).

Prior to formal assessment, all animals completed five habituation trials to minimize stress induced variability. Three consecutive test trials were then conducted, with a minimum of 5-minute rest between trials. The final motor performance score per animal was derived by summing the individual scores across all three evaluation domains.

Morris Water Maze Test

The Morris water maze apparatus comprised a circular, opaque pool (120 cm in diameter, 50 cm in depth) filled with water maintained at 24 ± 1°C via a thermostatically controlled heating system. A circular escape platform (10 cm in diameter) was submerged 1 cm beneath the water surface and permanently positioned at the center of a designated quadrant; its location remained constant and visually undetectable throughout all trials. During each trial, mice were gently placed into the water at a starting point located in the quadrant diagonally opposite the platform. The primary outcome parameter, escape latency, was defined as the time elapsed from release until the animal successfully climbed onto the hidden platform, serving as an index of spatial learning and memory retention. Trials were automatically terminated after 60 seconds if the platform was not found, and the maximum latency value (60 s) was recorded for that trial.

Open Field Test

The open field test is a well-established behavioral paradigm for assessing baseline locomotor activity and anxiety related responses in murine models, offering an indirect assessment of motor dysfunction in PD studies. The testing chamber is a square enclosure with floor markings delineating a central zone (20 m × 20 cm) and a surrounding peripheral zone. Mice were gently introduced into the center of the arena, and their spontaneous exploratory behavior was digitally recorded for 5 minutes using a computerized video tracking system.

Gait Analysis

The left and right forepaws were marked with red ink, while the hind paws were labeled with blue ink. Each mouse was carefully positioned at the starting end of a narrow, linear runway (90 cm long × 4.5 cm wide × 15 cm high), the floor of which was covered with plain white paper. Animals were gently prompted to walk unassisted to the opposite end, leaving behind a continuous trail of foodprints. Stride length was

calculated as the mean distance between successive imprints of the same forepaw (typically the left forepaw) across multiple consecutive steps.

4.11. Animal Materials and Processing

Tissue harvesting was conducted 24 hours following the final behavioral assessment. Prior to sacrifice, mice underwent a 12-hour fast (deprived of both food and water) and were then anesthetized with isoflurane inhalation. Retro-orbital blood collection was performed under stable anesthesia. Subsequently, animals were deeply anesthetized and subjected to transcranial perfusion via the left ventricle. For histological processing, a subgroup of mice received sequential perfusion with ice-cold phosphate-buffered saline (PBS), followed by 4% paraformaldehyde (PFA); brains were carefully extracted, post-fixed in 4% PFA at 4°C for 24 h, and processed for sectioning and staining. In parallel, another cohort underwent PBS only perfusion; their brains were rapidly excised on ice, and the striatum and substantia nigra were precisely dissected under cold conditions, snap frozen in liquid nitrogen, and stored at − 80°C until further analysis by biochemical or molecular techniques.

4.12. Nissl's Staining

Coronal brain sections from mice were subjected to toluidine blue staining, followed by progressive dehydration in an ascending ethanol series: two changes of 95% ethanol (5 min each), then two changes of absolute ethanol (10 min each). Subsequently, the sections were cleared in xylene (10 min) and permanently mounted onto glass slides using a nonaqueous, resin based mounting medium.

4.13. ELISA Assay

Concentrations of key immunomodulatory cytokines, namely TNF-α, IL-1β (pro-inflammatory), and TGF-β, IL-10 (anti-inflammatory), were measured in homogenized brain tissue samples via commercially available ELISA kits. All reagents were sourced from Shanghai Youxuan Biotechnology Co., Ltd. Assays were carried out strictly following the supplier’s standardized protocols, including recommended sample dilutions, incubation times, and detection procedures.

4.14. Proteomics Analysis

SNpc tissues were dissected from WT and BDNF cKO mice belonging to the MPTP and MPTP + Re treatment groups (n = 3 per group), immediately snap frozen in liquid nitrogen, and stored at − 80°C until proteomic profiling. Comprehensive quantitative proteomics was performed by Jingjie Biotechnology Co., Ltd. (Hangzhou, China). Briefly, total proteins were extracted from SNpc samples and quantified using the BCA method. Equal protein amounts were digested with sequencing grade trypsin under denaturing conditions. The resulting peptide mixtures were reconstituted in solvent A (0.1% formic acid in water) and separated via nanoflow liquid chromatography on a Vanquish Neo UPLC system. Peptides were ionized online using a nano electrospray source and analyzed by data independent acquisition (DIA) on a timsTOF HT mass spectrometer. Raw DIA files were processed with DIA-NN (v1.8), and spectra were searched against the ‘Mus musculus’ reference proteome (UniProt ID:

Mus_musculus_10090_SP_20241202.fasta; 17,236 canonical entries), supplemented with a reversed decoy database to estimate false discovery rates. Trypsin/P was specified as the digestion enzyme, permitting up to one missed cleavage. Fixed modifications included cysteine carbamidomethylating and N-terminal methionine removal. Peptide and protein level FDRs were both set at 1%. Protein abundances were normalized across runs and expressed as intensity based absolute quantification (iBAQ) like values; relative expression changes were calculated after median centering and $\log_2$ transformation. Proteins showing $|\log_2$ (fold change) $| > 0.263$ (i.e., > 1.2-fold change) and Benjamini Hochberg adjusted $p < 0.05$ were classified as differentially abundant. Functional interpretation, including GO term enrichment and KEGG pathway mapping, was conducted using the Jingjie Cloud bioinformatics platform.

4.15. Immunofluorescent (IF) Staining

Paraffin embedded midbrain sections containing the substantia nigra were subjected to standard deparaffinization and rehydration through a descending ethanol series (xylene, 100%, 95%, 75% ethanol), ending in distilled water. Antigen unmasking was achieved via heat induced epitope retrieval (HIER) using citrate buffer (pH 6.0) in a pressure cooker. A hydrophobic barrier was delineated around each tissue section using a PAP pen to confine reagents. Endogenous peroxidase activity was blocked with 3% H_2O_2 in methanol for 15 min, followed by incubation in 5% normal serum (species matched to the secondary antibody) for 1 h at room temperature to minimize nonspecific binding.

Primary antibodies, anti-tyrosine hydroxylase (TH; Proteintech, #25859-1-AP, 1:4000), anti-dopamine transporter (DAT; Proteintech, #22524-1-AP, 1:1000), anti-Iba1 (Servicebio, #GB113502, 1:5000), anti-CD86 (Servicebio, #GB150054, 1:2500), anti-CD206 (Servicebio, #GB115273, 1:4000), anti-occludin (Servicebio, #GB151401, 1:1000), anti-ZO-1 (Servicebio, #GB155686, 1:1000), and anti-NF-κB p65 (Servicebio, #GB11997, 1:1500), were applied individually and incubated overnight at 4°C. After washing, sections were incubated with species appropriate HRP conjugated secondary antibodies for 1 h at RT. Tyramide signal amplification (TSA) was performed using fluorophore conjugated tyramide reagent (diluted per manufacturer's specifications) for 10 min in darkness. To enable sequential multiplex labeling, bound antibodies were gently stripped using microwave assisted antigen retrieval (pH 9.0 buffer, 3 × 2 min pulses), preserving tissue morphology and epitope integrity. Following re-blocking, a second primary antibody was applied, followed by its matched HRP secondary and TSA development. This cycle was repeated as needed for multicolor detection. Nuclei were counterstained with DAPI (1 μg/mL) for 10 min. High resolution fluorescence images were acquired using a Nikon ECLIPSE C1 confocal microscope (Nikon, Tokyo, Japan). Fluorescence signal intensities within anatomically defined regions of interest (ROIs) were quantified using ImageJ (v1.54f) after background subtraction and standardized thresholding.

4.16. Immunoblotting Analysis

Striatal tissues from mice were lysed in ice-cold RIPA buffer containing freshly added protease and phosphatase inhibitor cocktails. Total protein concentration was quantified using a BCA protein assay

kit, and 20 μg of each sample was loaded per lane onto precast Tris-HCl polyacrylamide gels. Electrophoretic separation was performed under standard conditions, followed by electro transfer onto PVDF membranes. Membranes were blocked for 1 h at room temperature in 5% nonfat dry milk dissolved in TBST (Tris-buffered saline with 0.1% Tween-20). Primary antibodies, anti-α-syn (Selleck, #F0564, 1:1000), anti-TH (Proteintech, #25859-1-AP, 1:1000), anti-DAT (Proteintech, #22524-1-AP, 1:1000), anti-BDNF (Proteintech, #28205-1-AP, 1:1000), anti-TrkB (Proteintech, #13129-1-AP, 1:1000), anti-BAX (Proteintech, #50599-2-Ig, 1:1000), anti-cleaved caspase-3 (p17/p19; Proteintech, #19677-1-AP, 1:1000), anti-WDFY1 (Proteintech, #13960-1-AP, 1:1000), anti-TRIF/TICAM1 (ABclonal, #A13605, 1:5000), anti-STAT1 (ABclonal, #A12075, 1:1000), anti-Bcl-2 (ABclonal, #A0208, 1:2000), anti-phospho-NF-κB p65 (Ser529; HUABIO, #ET1604-27, 1:1000), anti-total NF-κB p65 (HUABIO, #ET1603-12, 1:1000), and anti-TLR4 (Zenbio, #505258, 1:500), were diluted in blocking buffer and incubated overnight at 4°C. After thorough washing, membranes were probed with HRP conjugated goat anti-rabbit IgG secondary antibody (1:5000) for 30 min at room temperature. Chemiluminescent signals were detected using the Tanon 5200 Multi fluorescent/chemiluminescent imaging system. Band intensities were normalized to corresponding β-actin or GAPDH loading controls and quantified via integrated optical density (IOD) analysis using ImageJ software (v1.54f), with background subtraction applied uniformly across all samples.

4.17. Co-Immunoprecipitation (Co-IP)

Tissues were homogenized in ice-cold Co-IP lysis buffer supplemented with a broad-spectrum protease inhibitor cocktail. Lysates were incubated on ice for 30 min with intermittent vertexing to ensure complete solubilization, followed by centrifugation at 11,000 × ‘g’ for 15 min at 4°C to pellet cellular debris. The clarified supernatant was collected, and total protein concentration was quantified using a BCA assay; samples were then normalized to a uniform concentration of 1 mg/mL (not 1000 mg/mL corrected unit). A 50 μL aliquot was reserved as the “input” control.

The remaining lysate was pre-cleared by adding 20 μL of Protein A/G magnetic beads (pre-equilibrated in lysis buffer), rotating gently for 1 h at 4°C, and removing beads magnetically. The pre-cleared lysate was split equally into two tubes. To one tube, 2 μg of anti-BDNF antibody (Santa Cruz, sc-65514) was added per 500 μg of total protein; the other tube received an equivalent amount (2 μg) of isotype matched mouse IgG control (Beyotime, A7028). Both were rotated overnight at 4°C. Subsequently, 30 μL of fresh Protein A/G magnetic beads were added to each sample and incubated for 2 h at 4°C under gentle rotation. Beads were then washed six times with cold IP lysis buffer to remove nonspecifically bound proteins. Immune complexes were eluted by resuspending beads in 30 μL of 1× SDS PAGE loading buffer and heating at 100°C for 10 min. Following magnetic separation, the supernatant containing the eluted antigen was collected and subjected directly to SDS PAGE and subsequent Western blot analysis.

4.18. Statistics Analysis

Statistical analyses were conducted using GraphPad Prism version 9.5. Data are presented as mean ± standard deviation (mean ± S.D.). Between group comparisons involving two independent conditions

were assessed using an unpaired, two tailed Student’s t test. For experiments with three or more experimental groups, one way analysis of variance (ANOVA) was applied, followed by the least significant difference (LSD) post hoc test for pairwise comparisons when the overall ANOVA yielded statistical significance ($p < 0.05$). A two-sided p value < 0.05 was deemed statistically significant.

Abbreviations

MPTP, 1-Methyl-4-phenyl-1,2,3,6-tetrahydropyridine.

MPP^+, 1-Methyl-4-phenylpyridinium ion.

α-Syn, Alpha-Synuclein.

BCL-2, B-cell leukemia/lymphoma-2.

Bax, Bcl-2 Associated X Protein.

BDNF, Brain Derived Neurotrophic Factor.

Cleaved Caspases3, Cleaved Cysteine Aspartate Specific Protease 3.

CD206, Cluster of Differentiation 206.

CD86, Cluster of Differentiation 86.

cKO, Conditional Knock Out.

DA, Dopamine.

DAT, Dopamine Transporter.

GsRe, Ginsenoside Re.

IL-1β, Interleukin-1 Beta.

IL-10, Interleukin-10.

Iba-1, Ionized Calcium Binding Adapter Molecule 1.

NF-κB, Nuclear Factor-kappa B.

p-NF-κB, Phosphorylated-Nuclear Factor-kappa B.

PD, Parkinson's Disease.

SNpc, Substantia Nigra Pars Compacta.

TRIF, TIR domain containing adapter molecule 1.

TLR4, Toll like receptor 4.

GS, Ginsenosides.

TGF-β, Transforming Growth Factor-Beta.

TrkB, Tropomyosin receptor kinase B.

TNF-α, Tumor Necrosis Factor-Alpha.

TH, Tyrosine Hydroxylase.

WDFY1, WD40 repeat and FYVE containing protein 1.

WT, Wild Type.

Declarations

Data Availability

The datasets generated and/or analyzed during the current study are not publicly available since related research is still in progress but are available from the corresponding author on reasonable request. The raw data and metadata are maintained on the following cloud platform (www.genescloud.cn), where the omics sequencing was performed.

Acknowledgments

The Shanghai Pujiang Program, China (grant number 23PJ1412300) as well as The Project of "Taking on Challenges and Accepting Responsibilities" of the Seventh People's Hospital of Shanghai University of Traditional Chinese Medicine (grant number QYCXZY250303).

CRediT Authorship Contribution Statement

M.T., F.Z. and Z.L. were responsible for drafting the initial manuscript. J.T. and D.G. contributed by offering editorial support, writing guidance, and valuable suggestions. The final version of the manuscript was reviewed and approved by J.G., W.G. and Z.Y. prior to submission. All authors played a role in the conception and submission of the manuscript.

Ethics Requirements

All experimental procedures involving animals were conducted in accordance with the guidelines approved by the Institutional Animal Care and Use Committee of Changchun University of Chinese Medicine (Ethics Approval Number: 2025929).

Competing Interest

The authors declare no competing interests.

Compliance with ARRIVE Guidelines

All animal experiments complied with the ARRIVE guidelines and were approved by the Institutional Animal Care and Use Committee of Changchun University of Chinese Medicine (Protocol Number: 2024299). Procedures followed national and international standards for animal welfare.

References

1. Morris, H.R., Spillantini, M.G., Sue, C.M. & Williams-Gray, C.H. The pathogenesis of Parkinson's disease. *The Lancet* **403**, 293-304 (2024).
2. Maguire-Zeiss, K.A. alpha-Synuclein: a therapeutic target for Parkinson's disease? *Pharmacol. Res.* **58**, 271-280 (2008).
3. Fabbri, M.*, et al.* Response of non-motor symptoms to levodopa in late-stage Parkinson's disease: Results of a levodopa challenge test. *Parkinsonism Relat. Disord.* **39**, 37-43 (2017).
4. Bawari, S.*, et al.* Targeting BDNF signaling by natural products: Novel synaptic repair therapeutics for neurodegeneration and behavior disorders. *Pharmacol. Res.* **148**, 104458 (2019).
5. Akbari, M.*, et al.* Expression of BDNF-Associated lncRNAs in Parkinson’s disease. *Metab. Brain Dis.* **37**, 901-909 (2022).
6. Miller, K.M.*, et al.* Striatal Afferent BDNF Is Disrupted by Synucleinopathy and Partially Restored by STN DBS. *J. Neurosci.* **41**, 2039-2052 (2021).
7. Kang, S.S.*, et al.* TrkB neurotrophic activities are blocked by α-synuclein, triggering dopaminergic cell death in Parkinson's disease. *Proc. Natl. Acad. Sci. U. S. A.* **114**, 10773-10778 (2017).
8. Palasz, E.*, et al.* BDNF as a Promising Therapeutic Agent in Parkinson’s Disease. *Int. J. Mol. Sci.* **21**, 1170 (2020).
9. Dluzen, D.E., Anderson, L.I., McDermott, J.L., Kucera, J. & Walro, J.M. Striatal dopamine output is compromised within +/- BDNF mice. *Synapse (New York, N.Y.)* **43**, 112-117 (2002).
10. Heidari, A., Yazdanpanah, N. & Rezaei, N. The role of Toll-like receptors and neuroinflammation in Parkinson’s disease. *J. Neuroinflammation* **19**, 135 (2022).
11. Conte, C.*, et al.* Toll Like Receptor 4 Affects the Cerebral Biochemical Changes Induced by MPTP Treatment. *Neurochem. Res.* **42**, 493-500 (2017).
12. Campolo, M.*, et al.* TLR4 absence reduces neuroinflammation and inflammasome activation in Parkinson’s diseases in vivo model. *Brain. Behav. Immun.* **76**, 236-247 (2019).
13. Meng, X.-w.*, et al.* Toll-like receptor-4/p38 MAPK signaling in the dorsal horn contributes to P2X4 receptor activation and BDNF over-secretion in cancer induced bone pain. *Neurosci. Res.* **125**, 37-45 (2017).

14. Rahimifard, M., *et al.* Targeting the TLR4 signaling pathway by polyphenols: A novel therapeutic strategy for neuroinflammation. *Ageing Res. Rev.* **36**, 11-19 (2017).
15. Muscat, S.M., *et al.* Selective TLR4 Antagonism Prevents and Reverses Morphine-Induced Persistent Postoperative Cognitive Dysfunction, Dysregulation of Synaptic Elements, and Impaired BDNF Signaling in Aged Male Rats. *J. Neurosci.* **43**, 155-172 (2023).
16. Bhattarai, Y., *et al.* Role of gut microbiota in regulating gastrointestinal dysfunction and motor symptoms in a mouse model of Parkinson's disease. *Gut Microbes* **13**, 1866974 (2021).
17. Munoz-Pinto, M.F., *et al.* Gut-first Parkinson's disease is encoded by gut dysbiome. *Mol. Neurodegener.* **19**, 78 (2024).
18. Hurley, M.J., *et al.* α-Synuclein expression in response to bacterial ligands and metabolites in gut enteroendocrine cells: an in vitro proof of concept study. *Brain Commun* **5**, fcad285 (2023).
19. Cheng, Y.K. & Chiang, H.S. The interrelationship between intestinal immune cells and enteric α-synuclein in the progression of Parkinson's disease. *Neurol. Sci.* **46**, 2965-2977 (2025).
20. de Castro Fonseca, M., Zanetti, L., Fanourakis, S., Sulzer, D.L. & Mazmanian, S.K. The gut microbiome, systemic inflammation, and autoimmunity in Parkinson's disease. *Lancet Neurol.* **25**, 103-114 (2026).
21. Ahn, E.H., *et al.* BDNF and Netrin-1 repression by C/EBPβ in the gut triggers Parkinson's disease pathologies, associated with constipation and motor dysfunctions. *Prog. Neurobiol.* **198**, 101905 (2021).
22. Choi, J.G., *et al.* Reduced Levels of Intestinal Neuropeptides and Neurotrophins in Neurotoxin-Induced Parkinson Disease Mouse Models. *J. Neuropathol. Exp. Neurol.* **80**, 15-20 (2021).
23. Lee, S.H., Jung, B.H., Kim, S.Y., Lee, E.H. & Chung, B.C. The antistress effect of ginseng total saponin and ginsenoside Rg3 and Rb1 evaluated by brain polyamine level under immobilization stress. *Pharmacol. Res.* **54**, 46-49 (2006).
24. Zhang, X., *et al.* Neuroprotective effects and mechanism of ginseng aqueous extract against Alzheimer's disease. *Phytomedicine* **153**, 157943 (2026).
25. Jiang, M., *et al.* Ginsenosides Rg1, Rb1 and rare ginsenosides: Promising candidate agents for Parkinson's disease and Alzheimer's disease and network pharmacology analysis. *Pharmacol. Res.* **212**, 107578 (2025).
26. Chen, H., *et al.* Ginsenoside Re Prevents Depression-like Behaviors via Inhibition of Inflammation, Oxidative Stress, and Activating BDNF/TrkB/ERK/CREB Signaling: An In Vivo and In Vitro Study. *J. Agric. Food Chem.* **72**, 19838-19851 (2024).
27. Liu, S., *et al.* Ginsenoside Re Inhibits NLRP3 Inflammasome Activation in Depressive Mice by Promoting PINK1-Mediated Mitophagy. *J. Agric. Food Chem.* **73**, 10934-10946 (2025).
28. Tang, X., *et al.* Ginsenoside Re inhibits non-small cell lung cancer progression by suppressing macrophage M2 polarization induced by AMPKα1/STING positive feedback loop. *Phytother. Res.* **38**, 5088-5106 (2024).

29. Wang, H.*, et al.* Ginsenoside Re protects against chronic restraint stress-induced cognitive deficits through regulation of NLRP3 and Nrf2 pathways in mice. *Phytother. Res.* **35**, 2523-2535 (2021).
30. Cai, J.S.*, et al.* A comprehensive system review of pharmacological effects and relative mechanisms of Ginsenoside Re: Recent advances and future perspectives. *Phytomedicine* **102**, 154119 (2022).
31. Li, J.*, et al.* Ginsenoside Re exerts neuroprotective in MPTP mice: potential links to gut microbiota and serum metabolism. *Neuropharmacology* **282**, 110596 (2026).
32. Zhou, S.*, et al.* Ginsenoside Rk3 Alleviates Neuroinflammation and Gastrointestinal Dysfunction in Parkinson's Disease via Modulation of Gut Microbiota-Mediated Butyric Acid Metabolism. *J. Agric. Food Chem.* **73**, 24139-24154 (2025).
33. Bindas, A.J., Kulkarni, S., Koppes, R.A. & Koppes, A.N. Parkinson's disease and the gut: Models of an emerging relationship. *Acta Biomater.* **132**, 325-344 (2021).
34. Li, X.*, et al.* Oral [60]fullerene reduces neuroinflammation to alleviate Parkinson's disease via regulating gut microbiome. *Theranostics* **13**, 4936-4951 (2023).
35. Mukhopadhya, I. & Louis, P. Gut microbiota-derived short-chain fatty acids and their role in human health and disease. *Nat. Rev. Microbiol.* **23**, 635-651 (2025).
36. Yang, X.*, et al.* Protective effect of ginsenoside CK against MPTP-induced Parkinson' s disease mouse model by suppressing oxidative stress and inflammation, and modulating the gut microbiota. *Microb. Pathog.* **202**, 107409 (2025).
37. Matin, S. & Dadkhah, M. BDNF/CREB signaling pathway contribution in depression pathogenesis: A survey on the non-pharmacological therapeutic opportunities for gut microbiota dysbiosis. *Brain Res. Bull.* **207**, 110882 (2024).
38. Cao, Y.*, et al.* Arbutin ameliorated depression by inhibiting neuroinflammation and modulating intestinal flora. *Phytomedicine* **145**, 156944 (2025).
39. Chen, Y.*, et al.* Semen Sojae Praeparatum alters depression-like behaviors in chronic unpredictable mild stress rats via intestinal microbiota. *Food Res. Int.* **150**, 110808 (2021).
40. Gorecki, A.M., Anyaegbu, C.C. & Anderton, R.S. TLR2 and TLR4 in Parkinson's disease pathogenesis: the environment takes a toll on the gut. *Transl Neurodegener* **10**, 47 (2021).
41. Zhang, R.*, et al.* TLR4/NF-κB signaling-mediated neuroinflammation is associated with gut microbiota dysbiosis in a mouse model of Parkinson's disease. *Front. Immunol.* **17**, 1672241 (2026).
42. Wu, J.*, et al.* Gut microbiota promote the propagation of pathologic α-syn from gut to brain in a gut-originated mouse model of Parkinson's disease. *Brain, Behavior, and Immunity* **128**, 152-169 (2025).
43. Lan, Y.*, et al.* Sea buckthorn polysaccharide ameliorates high-fat diet induced mice neuroinflammation and synaptic dysfunction via regulating gut dysbiosis. *Int. J. Biol. Macromol.* **236**, 123797 (2023).
44. Yuan, Y., Li, L., Nan, B., Yang, C.Y. & Yan, H.Y. Allicin Ameliorates Intestinal Barrier Damage via Microbiota-Regulated Short-Chain Fatty Acids-TLR4/MyD88/NF-κB Cascade Response in Acrylamide-Induced Rats. *J. Agric. Food Chem.* **69**, 12837-12852 (2021).

45. Yang, L.*, et al.* Astragaloside IV ameliorates Parkinson's disease by inhibiting TLR4/ NF-κB-dependent neuroinflammation. *Int. Immunopharmacol.* **160**, 114972 (2025).
46. Somensi, N.*, et al.* Role of toll-like receptor 4 and sex in 6-hydroxydopamine-induced behavioral impairments and neurodegeneration in mice. *Neurochem. Int.* **151**, 105215 (2021).
47. da Rocha Sobrinho, H.M.*, et al.* TLR4 and TLR2 activation is differentially associated with age during Parkinson's disease. *Immunol. Invest.* **47**, 71-88 (2018).
48. Hughes, C.D.*, et al.* Picomolar concentrations of oligomeric alpha-synuclein sensitizes TLR4 to play an initiating role in Parkinson's disease pathogenesis. *Acta Neuropathol.* **137**, 103-120 (2019).
49. Cheng, Z., Taylor, B., Ourthiague, D.R. & Hoffmann, A. Distinct single-cell signaling characteristics are conferred by the MyD88 and TRIF pathways during TLR4 activation. *Sci. Signal.* **8**, ra69 (2015).
50. Bellucci, A.*, et al.* Nuclear Factor-κB Dysregulation and α-Synuclein Pathology: Critical Interplay in the Pathogenesis of Parkinson's Disease. *Front. Aging Neurosci.* **12**, 68 (2020).
51. Xiong, L.*, et al.* Design and synthesis of novel derivatives of bisepoxylignans as potent anti-inflammatory agents involves the modulation of the M1/M2 microglia phenotype via TLR4/NF-κB signaling pathway. *Eur. J. Med. Chem.* **282**, 117092 (2025).
52. Choi, S.E., Park, Y.S. & Koh, H.C. NF-κB/p53-activated inflammatory response involves in diquat-induced mitochondrial dysfunction and apoptosis. *Environ. Toxicol.* **33**, 1005-1018 (2018).
53. Nociti, V. & Romozzi, M. The Role of BDNF in Multiple Sclerosis Neuroinflammation. *Int. J. Mol. Sci.* **24**, 8447 (2023).
54. Huang, D.*, et al.* Brain-specific NRSF deficiency aggravates dopaminergic neurodegeneration and impairs neurogenesis in the MPTP mouse model of Parkinson's disease. *Aging (Albany N. Y.)* **11**, 3280-3297 (2019).
55. Boger, H.A.*, et al.* Effects of brain-derived neurotrophic factor on dopaminergic function and motor behavior during aging. *Genes, Brain Behav.* **10**, 186-198 (2011).
56. Rantamaki, T.*, et al.* The Impact of Bdnf Gene Deficiency to the Memory Impairment and Brain Pathology of APPswe/PS1dE9 Mouse Model of Alzheimer's Disease. *PLoS One* **8**, e68722 (2013).
57. Li, H.*, et al.* Pro-BDNF Knockout Causes Abnormal Motor Behaviours and Early Death in Mice. *Neuroscience* **438**, 145-157 (2020).
58. Wu, S.Y.*, et al.* BDNF reverses aging-related microglial activation. *J. Neuroinflammation* **17**, 210 (2020).
59. Bi, C.L., Fu, Y.L. & Li, B. Brain-derived neurotrophic factor alleviates diabetes mellitus-accelerated atherosclerosis by promoting M2 polarization of macrophages through repressing the STAT3 pathway. *Cell. Signal.* **70**, 109569 (2020).
60. Lindqvist, D.*, et al.* Cerebrospinal fluid inflammatory markers in Parkinson's disease - Associations with depression, fatigue, and cognitive impairment. *Brain, Behavior, and Immunity* **33**, 183-189 (2013).

61. Kovler, M.L.*, et al.* Toll-like receptor 4-mediated enteric glia loss is critical for the development of necrotizing enterocolitis. *Sci. Transl. Med.* **13**, eabg3459 (2021).
62. Zhou, J.B., Wang, M.C. & Deng, D.F. KLF2 protects BV2 microglial cells against oxygen and glucose deprivation injury by modulating BDNF/TrkB pathway. *Gene* **735**, 144277 (2020).
63. Hu, Y.-H.*, et al.* WDFY1 mediates TLR3/4 signaling by recruiting TRIF. *EMBO Rep.* **16**, 447-455 (2015).
64. Li, D.*, et al.* Grass carp (Ctenopharyngodon idella) WDFY1 activates IFN1 response via TLR3-TRIF-IRF3 axis. *Fish Physiol. Biochem.* **51**, 131 (2025).
65. Ning, F.*, et al.* Hes1 attenuates type I IFN responses via VEGF-C and WDFY1. *J. Exp. Med.* **216**, 1396-1410 (2019).
66. Sancho-Balsells, A.*, et al.* Lack of Helios During Neural Development Induces Adult Schizophrenia-Like Behaviors Associated With Aberrant Levels of the TRIF-Recruiter Protein WDFY1. *Front. Cell. Neurosci.* **14**, 93 (2020).
67. Nair, A. & Jacob, S. A simple practice guide for dose conversion between animals and human. *Journal of Basic and Clinical Pharmacy* **7**, 27-31 (2016).

Table

Table is available in the Supplementary Files section.

Figures

Figure 1

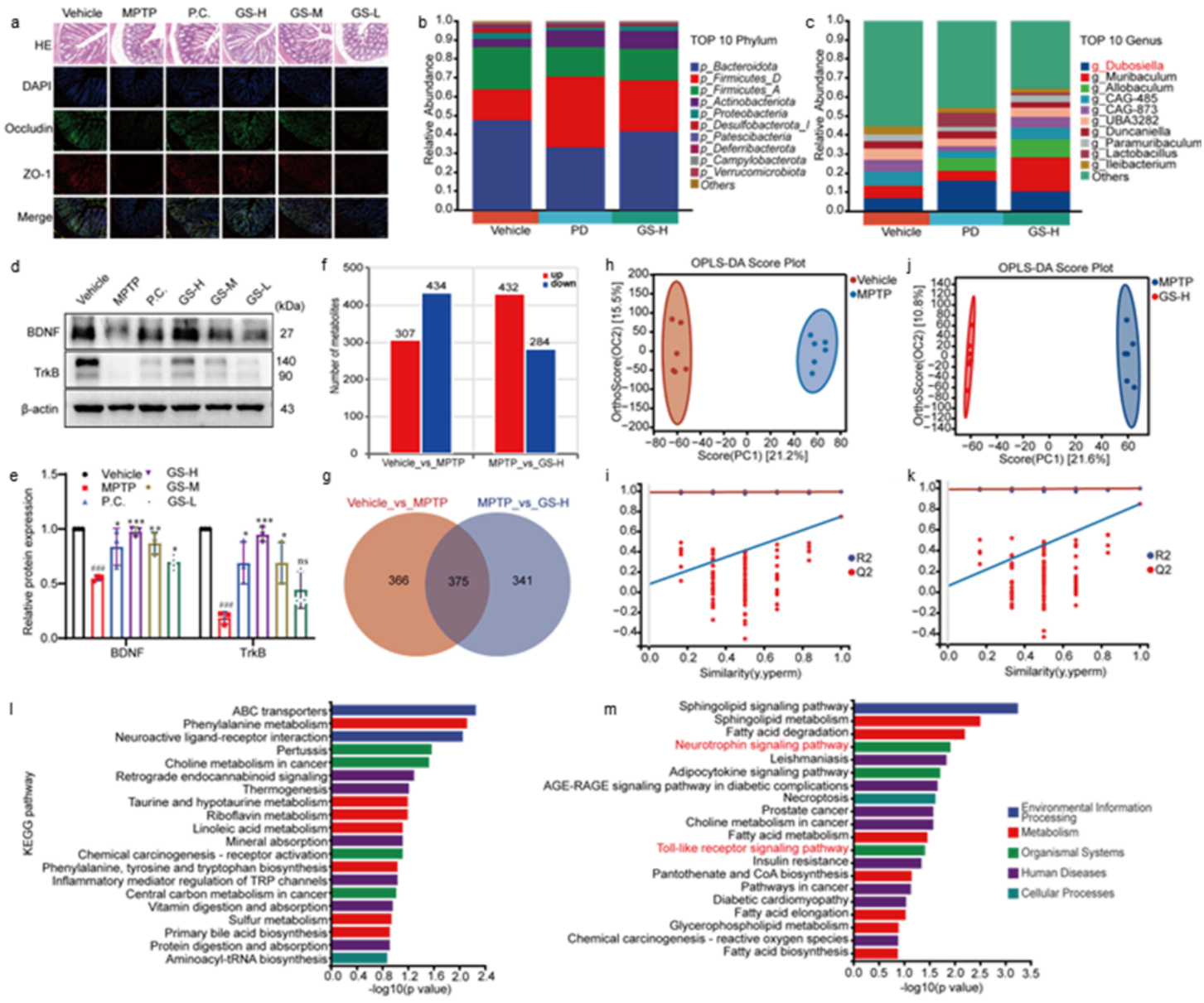

Figure 1

Data are presented as mean ± S.D. One way ANOVA was used for comparisons among multiple groups. Statistical significance: $^{\#}p < 0.05$, $^{\#\#}p < 0.01$, $^{\#\#\#}p < 0.001$ vs. Vehicle group; $^{*}p < 0.05$, $^{**}p < 0.01$, $^{***}p < 0.001$ vs. MPTP group.

GS ameliorate MPTP induced intestinal pathological damage, gut microbiota dysbiosis, and metabolite imbalance in a mouse model of PD.

(a) Histological analysis of colon tissues: H&E staining (scale bar: 100 μm; magnification: 20×) showing intestinal morphology. Immunofluorescence staining for tight junction proteins OCCLUDIN and ZO-1 (scale bar: 100 μm; magnification: 20×) with quantitative analysis of fluorescence intensity (n=3).

(b) Relative abundance of gut microbiota at the phylum level.

(c) Relative abundance of gut microbiota at the genus level.

(d–e) Western blot analysis of BDNF and TrkB protein expression in mouse striatal tissue (d) with densitometric quantification normalized to a loading control (e; n=3).

(f) Volcano plot (or bar chart, as applicable) showing differential fecal metabolites between experimental groups.

(g) Venn diagram illustrates the overlap of differential metabolites between the Vehicle vs. MPTP groups and MPTP vs. GS groups.

(h–i) Orthogonal partial least squares discriminant analysis (OPLS-DA) score plot (h) and permutation test (i) of fecal metabolites comparing the Vehicle and MPTP groups.

(j–k) OPLS-DA score plot (j) and permutation test (k) of fecal metabolites comparing the MPTP and GS groups.

(l) KEGG pathway enrichment analysis of differential metabolites between the Vehicle and MPTP groups.

(m) KEGG pathway enrichment analysis of differential metabolites between the MPTP and GS-H (high dose GS) groups.

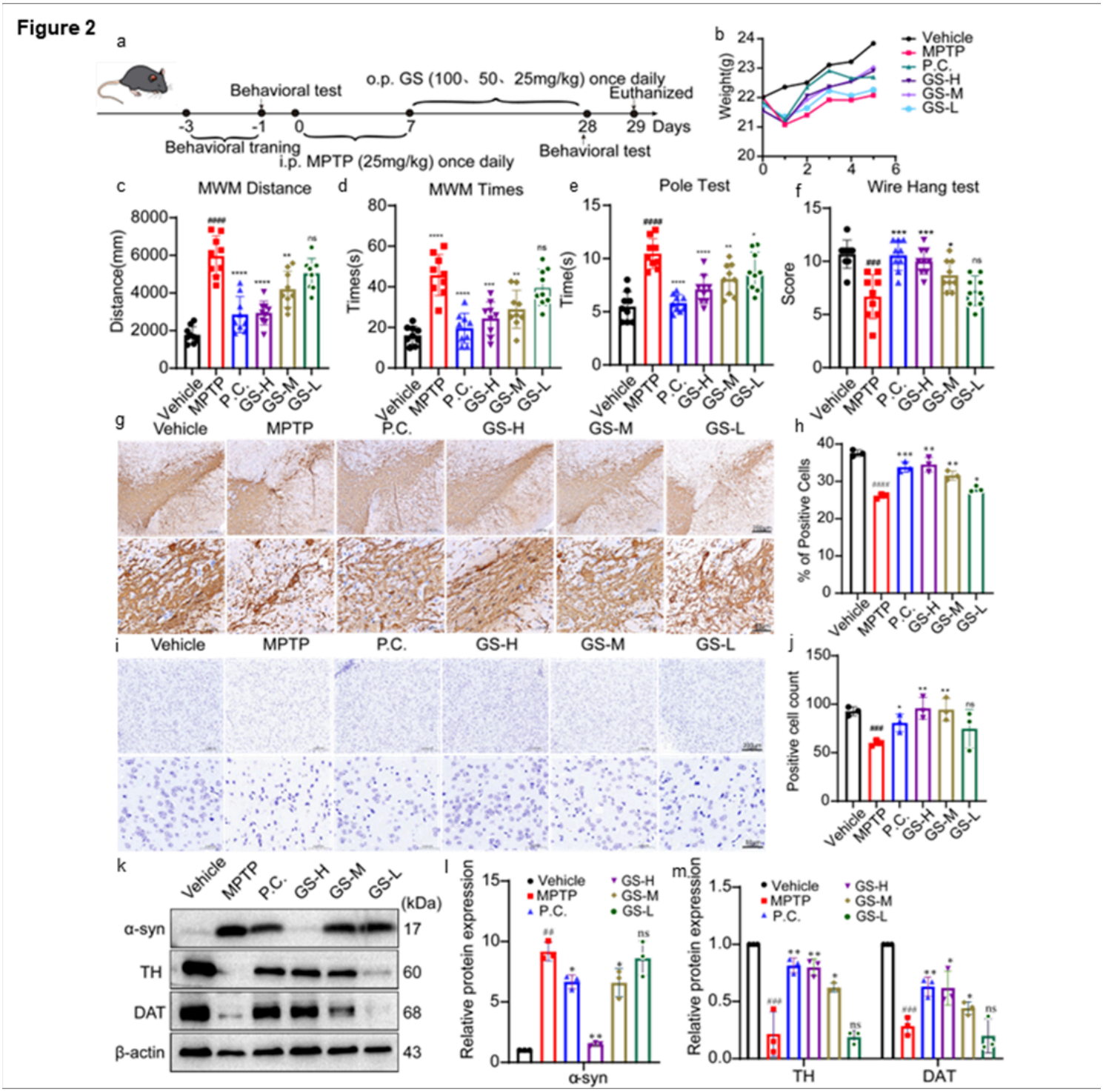

Figure 2

GS ameliorates motor dysfunction and pathological damage in MPTP induced mouse models of PD.

(a) Schematic overview of animal experimental design.

(b) Time course changes in body weight of mice (n=9 per group).

(c–d) Morris's water maze test: total swimming distance (c) and escape latency to the hidden platform (d) (n=9 per group).

(e) Latency to descend the pole in the pole climbing test (n=9 per group).

(f) Quantitative analysis of hanging wire test scores (n=9 per group).

(g–h) Nissl staining of striatal sections: representative images (g) and quantification of Nissl positive neuronal areas (h) (n=3 per group; scale bar: 50 μm; magnification: 40×).

(i–j) IHC staining of the SNpc: representative images (i) and quantification of TH positive dopaminergic neurons (j) (n=3 per group; scale bar: 50 μm; magnification: 40×).

(k–m) Western blot analysis of α-syn, TH, and DAT protein expression in brain tissues: representative blots (k) and densitometric quantification normalized to a loading control (l–m) (n=3 per group).

Data are presented as mean ± S.D. One way ANOVA was used for comparisons among multiple groups. Statistical significance: $^{\#}p < 0.05$, $^{\#\#}p < 0.01$, $^{\#\#\#}p < 0.001$ vs. Vehicle group; $^{*}p < 0.05$, $^{**}p < 0.01$, $^{***}p < 0.001$ vs. MPTP group.

Figure 3

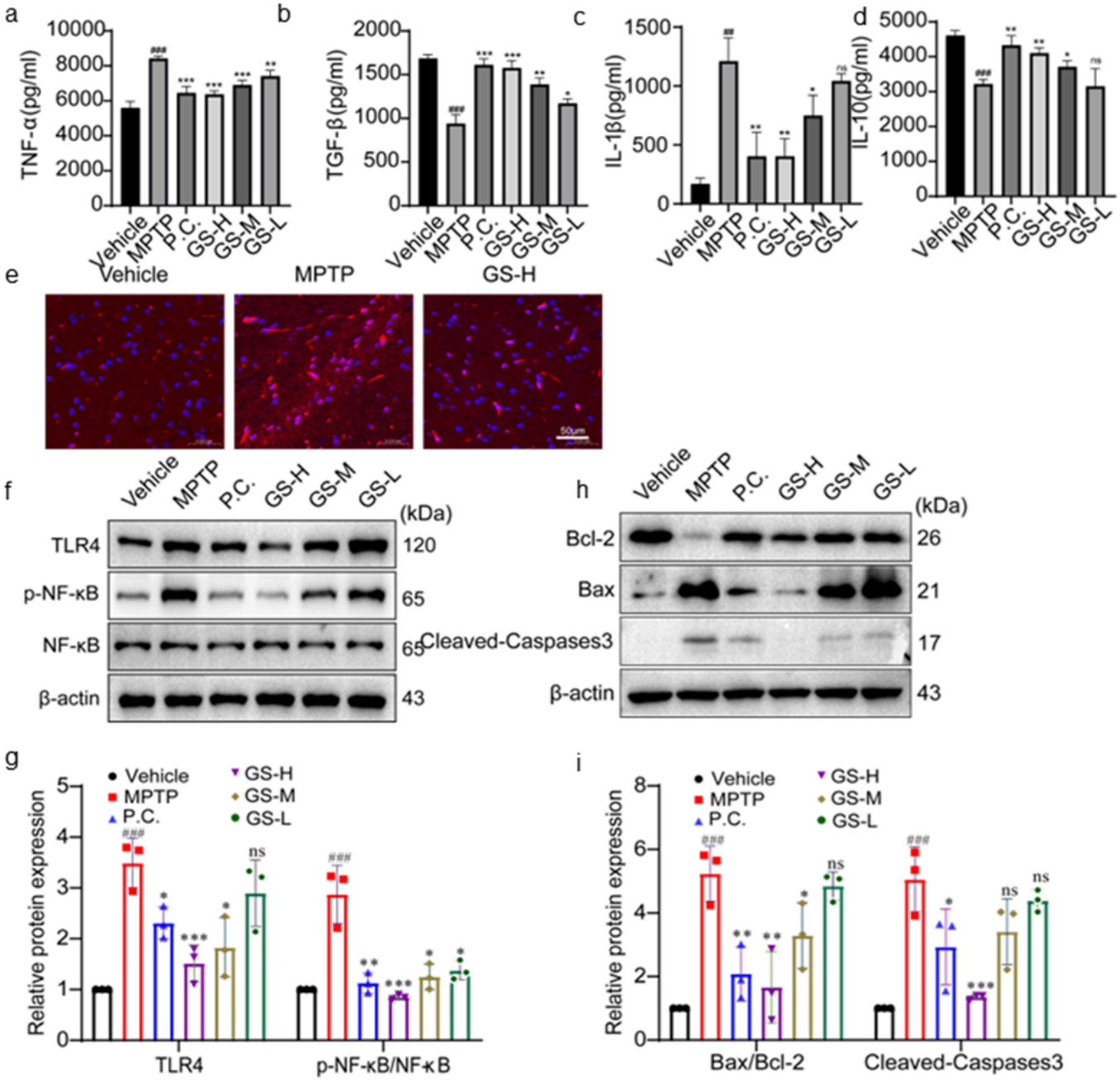

Figure 3

GS inhibits MPTP induced neuroinflammation, neuronal apoptosis, and activation of the TLR4/NF-κB axis in PD mouse models.

(a–d) ELISA quantification of pro-inflammatory (TNF-α, IL-1β) and anti-inflammatory (TGF-β, IL-10) cytokine levels in mouse brain tissue (n=6 per group).

(e) IF staining showing NF-κB nuclear translocation (scale bar: 50 μm; magnification: 40×; n=3 per group).

(f–g) Western blot analysis of TLR4, total NF-κB, and NF-κB phosphorylated at Ser529 (p-NF-κB Ser529): representative blots (f) and densitometric quantification normalized to a loading control (g) (n=3 per group).

(h–i) Western blot analysis of apoptosis related proteins (anti-apoptotic Bcl-2, pro-apoptotic Bax, and cleaved caspase-3): representative blots (h) and densitometric quantification normalized to a loading control (i) (n=3 per group).

Data are presented as mean ± S.D. One way ANOVA was used for comparisons among multiple groups. Statistical significance: $^{\#}p < 0.05$, $^{\#\#}p < 0.01$, $^{\#\#\#}p < 0.001$ vs. Vehicle group; $^{*}p < 0.05$, $^{**}p < 0.01$, $^{***}p < 0.001$ vs. MPTP group.

Figure 4

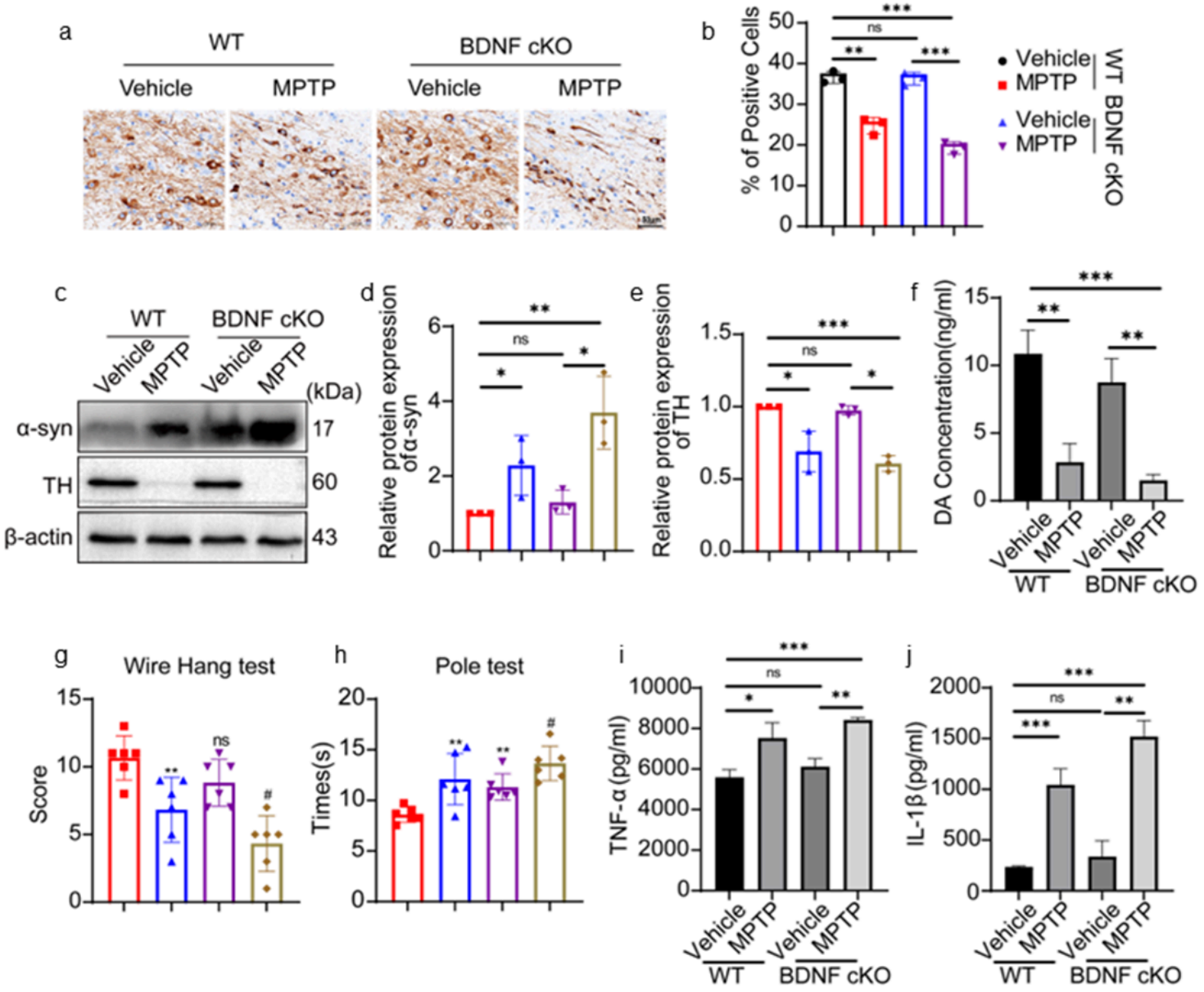

Figure 4

BDNF deficiency exacerbates pathological progression and neuroinflammation in PD models.

(a–b) IHC staining of the SNpc: representative images (a) and quantification of TH positive dopaminergic neurons (b) (n=3 per group; scale bar: 50 μm; magnification: 40×).

(c–d) Western blot analysis of α-syn and TH protein expression: representative blots (c) and densitometric quantification normalized to a loading control (d) (n=3 per group).

(e) ELISA based measurement of striatal dopamine content (n=6 per group).

(f) Quantitative analysis of hanging wire test scores (n=9 per group).

(g) Latency to descend the pole in the pole climbing test (n=9 per group).

(h–i) ELISA quantification of pro-inflammatory cytokines TNF-α (h) and IL-1β (i) in mouse brain tissue (n=6 per group).

Data are presented as mean ± S.D. Student's two tailed t test was employed for two group comparisons. Statistical significance: $^{*}p < 0.05$, $^{**}p < 0.01$, $^{***}p < 0.001$ (group comparisons as indicated by experimental design).

Figure 5

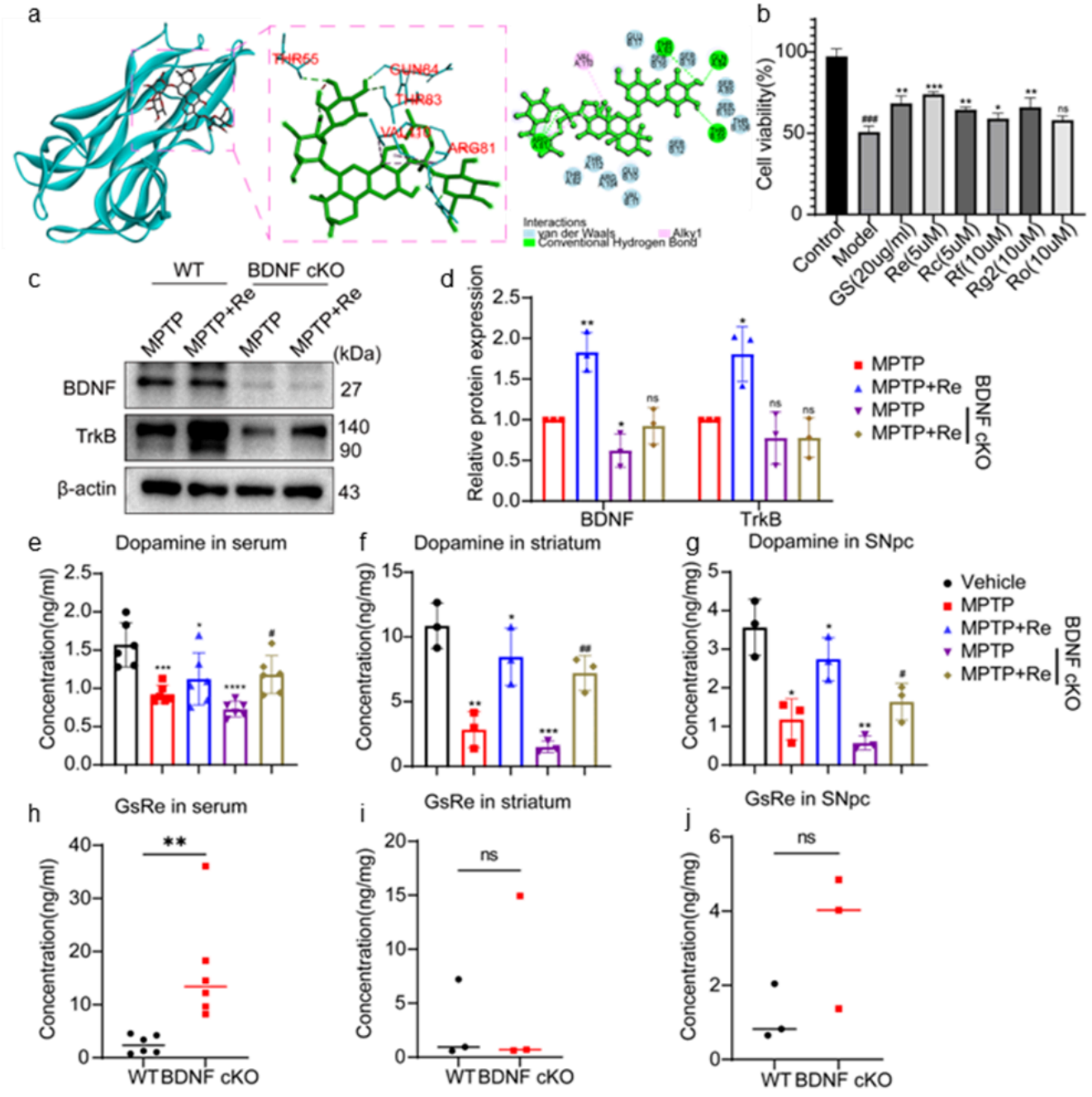

Figure 5

GsRe, a key component of GS, crosses the BBB and regulates BDNF levels.

(a) Molecular docking visualization of GsRe binding to BDNF, with a calculated docking binding energy of -7.4 kcal/mol.

(b) CCK-8 assay evaluating the protective effects of different GS on MPP^+ induced neuronal cell viability (n=3 per group).

(c–d) Western blot analysis of BDNF and TrkB protein expression: representative blots (c) and densitometric quantification normalized to a loading control (d) (n=3 per group).

(e–g) UPLC-MS/MS quantification of dopamine content in serum (e), striatum (f), and SNpc (g) (n=6 per group).

(h–j) UPLC-MS/MS quantification of GsRe levels in serum (h), striatum (i), and SNpc (j) (n=6 per group).

Data are presented as mean ± S.D. Student's two tailed t test was employed for two group comparisons. One way ANOVA was used for comparisons among multiple groups. Statistical significance: $^{*}p < 0.05$, $^{**}p < 0.01$, $^{***}p < 0.001$ (group comparisons as indicated by experimental design).

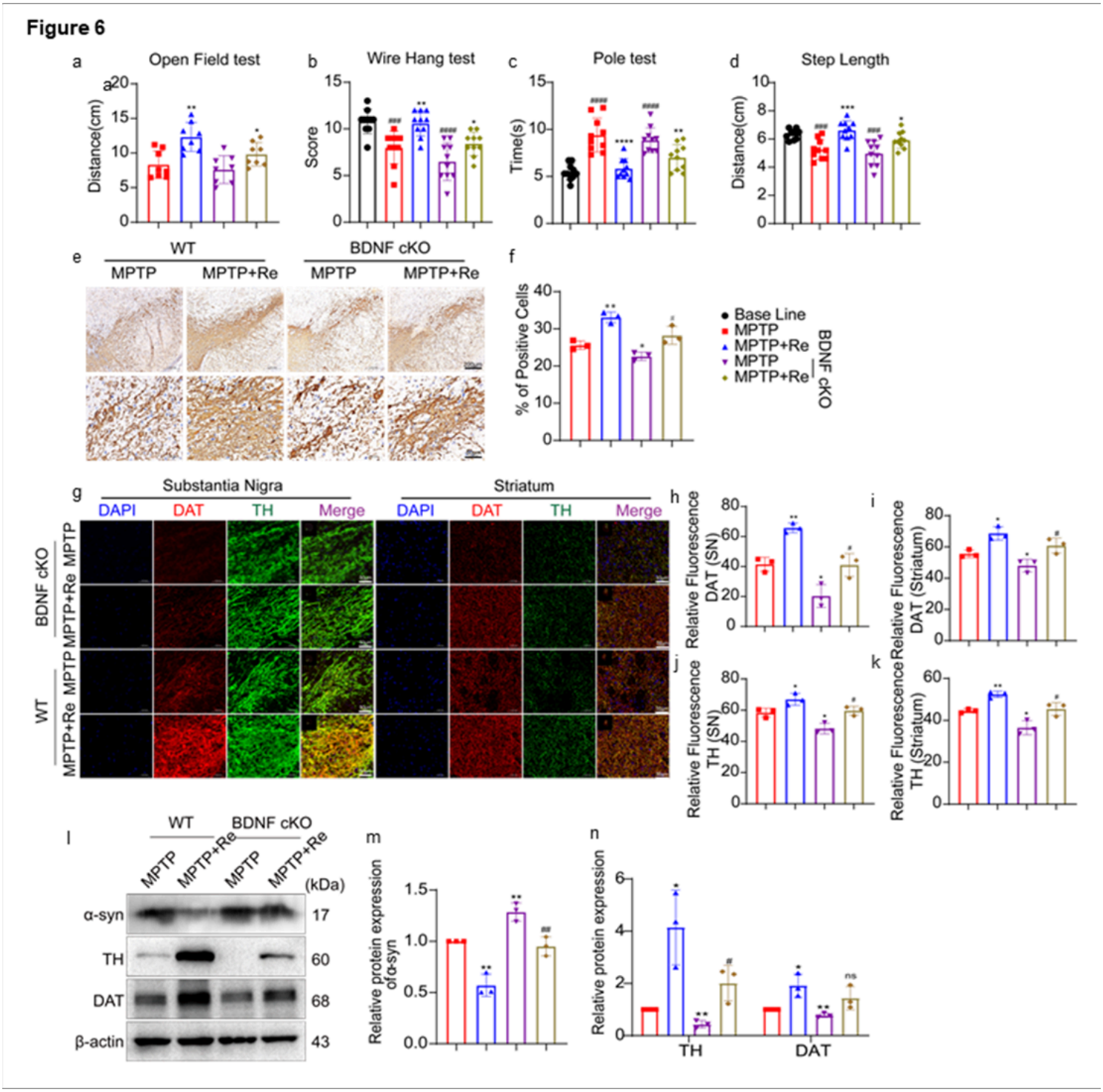

Figure 6

GsRe ameliorates motor dysfunction and dopaminergic neuron loss in PD mouse models.

(a) Total distance traveled within 5 minutes in the open field test (n=9 per group). (b) Stride length of mice (n=9 per group).

(c) Latency to descend the pole in the pole climbing test (n=9 per group).

(d) Hanging wire test score (n=9 per group).

(e–f) IHC staining of the SNpc: representative images (e) and quantification of TH positive dopaminergic neurons (f) (n=3 per group; scale bar: 50 μm; magnification: 40×).

(g–k) IF staining for TH and DAT in the SNpc and striatum: representative images and quantification of TH/DAT positive signals (n=3 per group; scale bar: 50 μm; magnification: 40×).

(l–n) Western blot analysis of α-syn, TH, and DAT protein expression: representative blots (l) and densitometric quantification normalized to a loading control (m-n) (n=3 per group).

Data are presented as mean ± S.D. Student's two tailed t test was employed for two group comparisons. Statistical significance: $^{*}p < 0.05$, $^{**}p < 0.01$, $^{***}p < 0.001$ vs. MPTP group; $^{\#}p < 0.05$, $^{\#\#}p < 0.01$ vs. BDNF cKO + MPTP group; ns: no statistical significance.

Figure 7

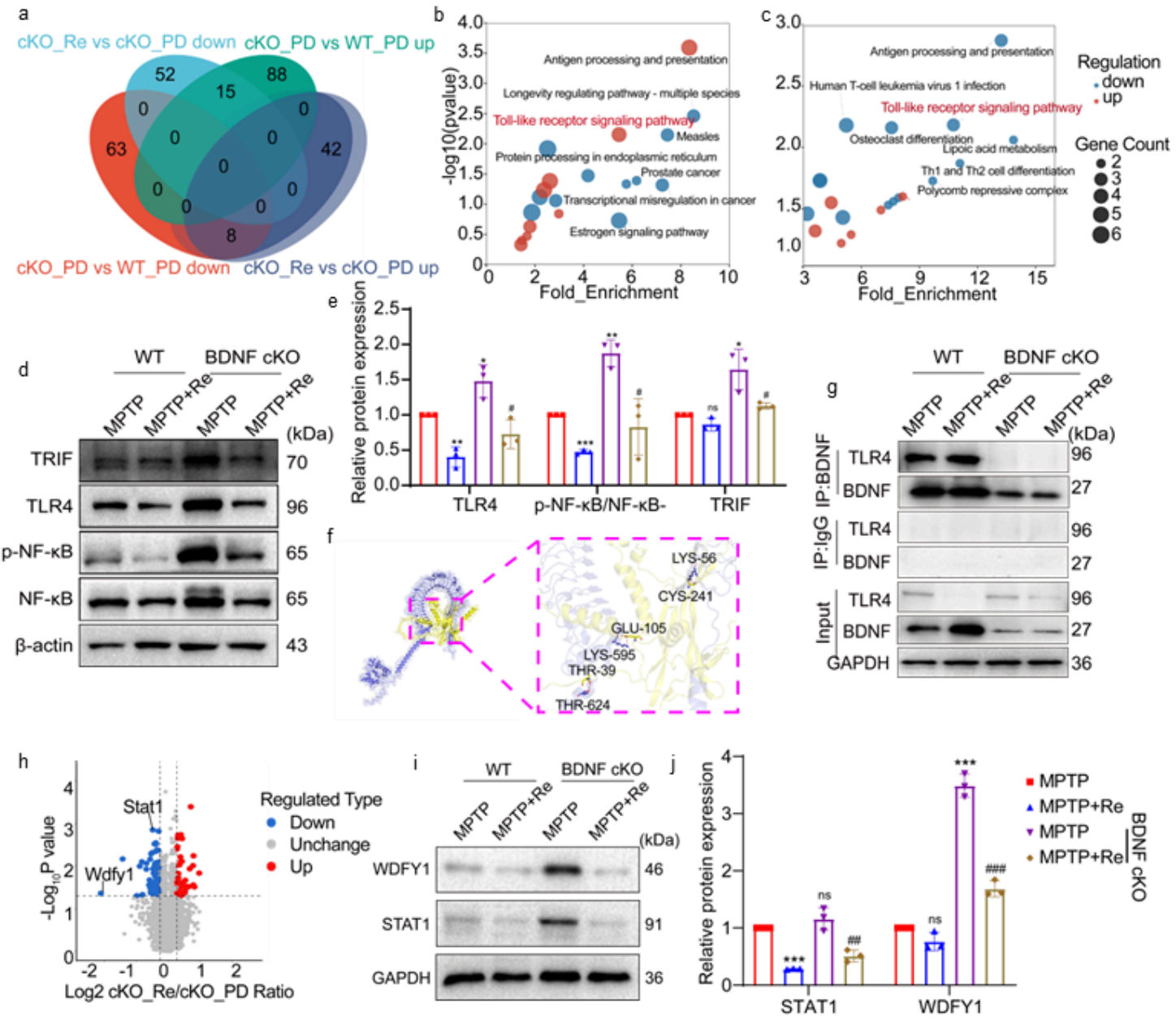

Figure 7

Proteomics analysis reveals GsRe alleviates BDNF mediated TLR signaling pathway activation in PD models.

(a) Venn diagram illustrates the overlap of upregulated and downregulated DEPs between two comparison pairs: BDNF cKO + MPTP vs. WT + MPTP, and BDNF cKO + MPTP vs. BDNF cKO + GsRe (n=3 per group).

(b) KEGG pathway enrichment analysis of DEPs in the BDNF cKO + MPTP vs. WT + MPTP group.

(c) KEGG pathway enrichment analysis of DEPs in the BDNF cKO + GsRe vs. BDNF cKO + MPTP group.

(d–e) Western blot analysis of TLR4, TRIF, NF-κB, and p-NF-κB protein expression: representative blots (d) and densitometric quantification normalized to a loading control (e) (n=3 per group).

(f) Molecular docking visualization of BDNF/TLR4 interaction, with a calculated docking binding energy of -20.5 kcal/mol.

(g) Co-IP assay verifying the PPI between BDNF and TLR4 (n=3 per group).

(h) Volcano plot of DEPs in the BDNF cKO + GsRe vs. BDNF cKO + MPTP group (n=3 per group).

(i–j) Western blot analysis of WDFY1 and STAT1 protein expression: representative blots (i) and densitometric quantification normalized to a loading control (j) (n=3 per group).

Data are presented as mean ± S.D. Student's two tailed t test was employed for two group comparisons. Statistical significance: $^{*}p < 0.05$, $^{**}p < 0.01$, $^{***}p < 0.001$ vs. MPTP group; $^{\#}p < 0.05$, $^{\#\#}p < 0.01$ vs. BDNF cKO + MPTP group; ns: no statistical significance.

Figure 8

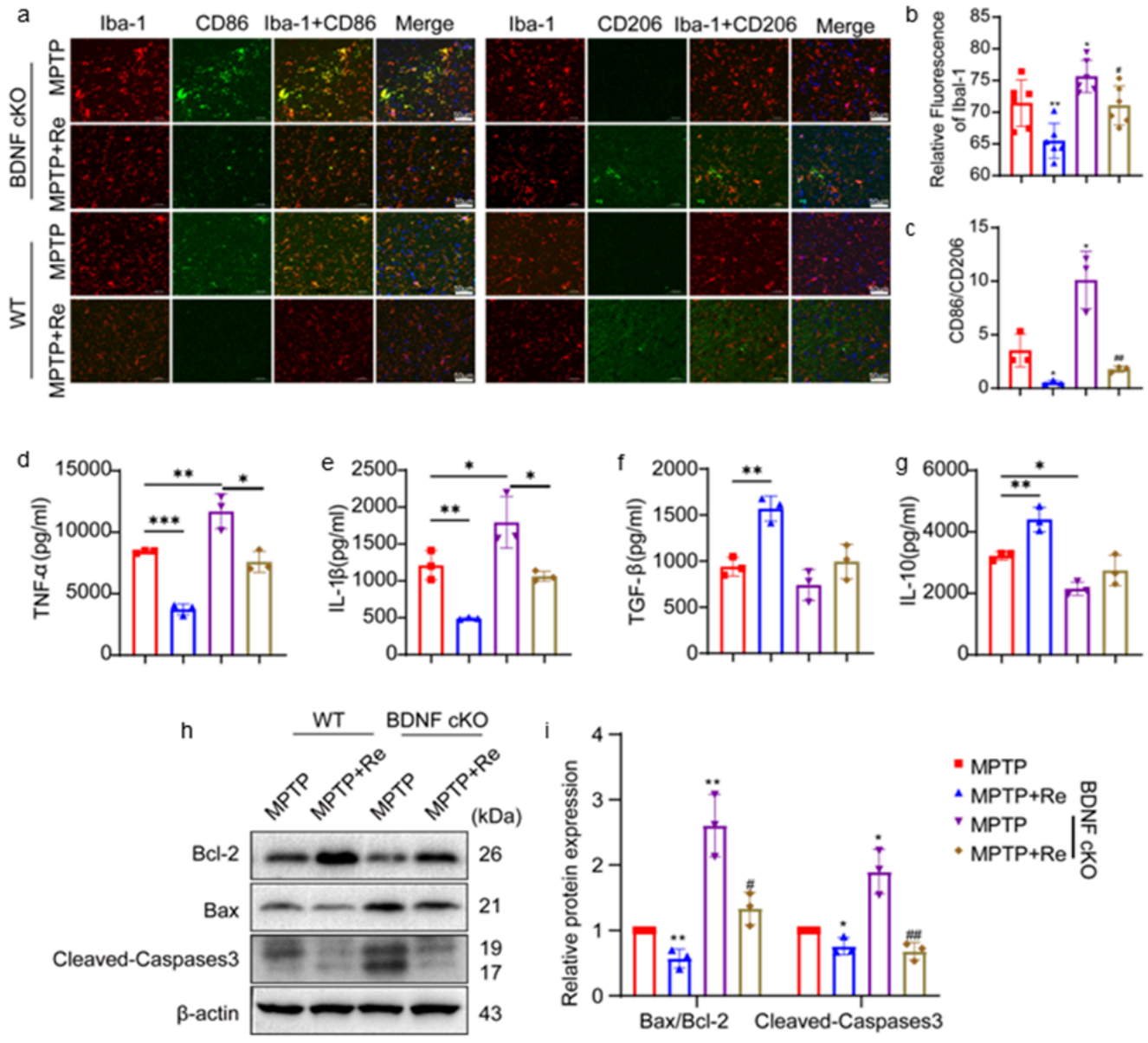

Figure 8

GsRe inhibits TLR4 mediated neuroinflammation, microglial polarization, and neuronal apoptosis in PD mouse models.

(a) Representative images of double IF staining for Iba-1⁺/CD86⁺ (M1 pro-inflammatory microglia) and Iba-1⁺/CD206⁺ (M2 anti-inflammatory microglia) cells (n=3 per group; scale bar: 50 μm, magnification: 40×).

(b) Quantitative analysis of MFI of Iba-1 (microglial activation marker) in brain tissue (n=6 per group).

(c) Ratio of MFI of CD86 to CD206 (n=3 per group).

(d–g) ELISA measurement of pro-inflammatory cytokines TNF-α (d) and IL-1β (e), and anti-inflammatory cytokines TGF-β (f) and IL-10 (g) in mouse brain tissue (n=3 per group).

(h–i) Western blot analysis of apoptosis related proteins: Bcl-2, Bax, and cleaved caspase-3 (h) and densitometric quantification normalized to a loading control (i) (n=3 per group).

Data are presented as mean ± S.D. Student's two tailed t test was employed for two group comparisons. Statistical significance: $^{*}p < 0.05$, $^{**}p < 0.01$, $^{***}p < 0.001$ vs. MPTP group; $^{\#}p < 0.05$, $^{\#\#}p < 0.01$ vs. BDNF cKO + MPTP group; ns: no statistical significance.

Supplementary Files

This is a list of supplementary files associated with this preprint. Click to download.

- Table.docx
- OriginalWesternBlots.pptx
- Graphicalabstract.tif
- SupplementaryFigure1.tif
- SupplementaryFigure7.tif
- SupplementaryFigure2.tif
- SupplementaryFigure3.tif
- SupplementaryFigure4.tif
- SupplementaryFigure5.tif
- SupplementaryFigure6.tif
- SupplementaryFigure8.tif